MÖSSBAUER EFFECT STUDIES IN YTTRIUM BASED METALLIC GLASSES

Thesis by

Michael A. Tenhover

In Partial Fulfillment of the Requirements

for the Degree of

Doctor of Philosophy

California Institute of Technology

Pasadena, California

1981

(Submitted April 29, 1981)

To my Father

ACKNOWLEDGEMENTS

I am pleased to acknowledge the valuable support of Professor W.L. Johnson and Professor Pol Duwez in this work. I am especially grateful to Professor W.L. Johnson for giving me the opportunity to pursue my own special interests in amorphous materials and for his support and encourgement of my work. My relationship with him has helped my development both as a scientist and as a person. A special thanks to Professor P. Boolchand who sparked my interest in amorphous materials and Mössbauer Effect. I have benefited from discussions with many fine scientists,especially C.C. Tsuei, J. Bevk, F. Spaepen, F. Habbal, H. Freyhardt, and U. Koster. I wish to thank W. Bresser for his help with some of the DSC measurements and A. Williams for his assistance with data processing and the use of his celebrated Tape/Card program. A very special thanks to M. Imaeda. On the technical side, I wish to acknowledge the excellent support I have received from C. Geremia, S. Kotake, J. Wysocki, and A. Bressan. Support for this work came from the U.S. Department of Energy and the International Business Machines Corporation.

ABSTRACT

The short range order of a variety of Yttrium-3d transition metal glasses has been investigated using Fe^{57} Mössbauer Effect (ME) spectroscopy. We found that the ME spectra of these glasses could best be described in terms of a model which assumes two kinds of sites for the 3d elements. The nature of the two sites is radically different depending on whether the transition metal is Mn, Fe, Co, and Ni or Cu and Zn. We attributed the difference in the structure of these glasses to the same factors which determine whether a C-15 crystalline compound is stable in equilibrium. The microscopic nature of ME spectroscopy provides an interesting comparison between the nature of the short range order in crystalline and amorphous alloys. The process of crystallization has also been studied for a few glasses, and was found to occur in two distinct steps associated with the formation of hcp Y and a C-15 compound. In the final section we use the results of this study to design a novel high field superconducting material.

TABLE OF CONTENTS

LIST OF TABLES

LIST OF FIGURES

I. INTRODUCTION

Amorphous materials have been known to mankind since ordinary glass was found in the Middle East some 6000 years ago.[1] Since that time a wide variety of amorphous materials have been fabricated and investigated. Examples of amorphous materials can be found within all classifications of solids. There are metallic, covalent, ionic, and even Van der Waals amorphous solids. Each of these types of amorphous materials has a characteristic requirement which determines the local atomic structure. The structure of amorphous Si, for example, is governed by the need of each Si atom to form four directional bonds so that its structure is a tetrahedral continuous random network. In this work, we are interested in the local atomic structure of amorphous metals. Amorphous metals can be prepared by a number of techniques, such as electrodeposition, chemical vapor deposition, sputtering, and evaporation. These methods of preparation usually result in very thin samples of frequently poorly defined composition. An important discovery in the area of amorphous metals was made by Duwez et al[2] at Caltech in the late 1950's. They found that certain metallic alloys could be transformed into a non-crystalline state by quenching from the liquid. The compositions of these metallic glasses, as they were later called, was found to lie near a eutectic composition where the liquid phase is most stable compared to the solid. The metallic glasses they were producing are now known as metal-metalloid glasses since they consisted of late transition metals (Pd, Ni, Fe...) and one or more metalloid

atoms (B, P, Si, ...). Since that time, metallic glasses have been found in many other types of metallic alloys. In addition to metal-metalloid glasses (e.g. $Pd_{80}Si_{20}$), there are early transition metal-late transition metal glasses, rare earth-late transition metal glasses, and even Actinide-transition metal glasses. The importance of the discovery of Duwez et al is that it resulted in a surge of interest in amorphous metallic solids. It is becoming apparent that many of these materials are going to have important technological applications. Some of the metal-metalloid glasses (e.g. $Fe_{80}B_{20}$) are being considered for use in magnetic devices such as power transformers. The rare earth-late transition metal amorphous alloys (e.g. Gd-Fe) are possible constituents of computer memories in the form of magnetic bubble devices and may find use in the area of magnetic recording. A second reason for the interest in these materials is that they opened up a completely new field of research. Metallic glasses, fabricated by the techniques of Duwez et al, have permitted experiments which would be difficult if not impossible on thin film materials. Our understanding of non-crystalline materials has therefore been greatly enhanced by the advent of metallic glasses.

The structure of metallic glasses has been a subject of great interest. Most of the information we have on the arrangements of atoms in these materials has come from the various diffraction techniques (electron, X-ray, and neutron diffraction).[3] In addition to this, some extended X-ray absorption fine structure (EXAFS) studies have been reported on a number of metallic glasses.[4,5] The object of all these

experiments is to determine the pair correlation functions $\rho_{ij}(r)$ which contain information on the number of j-type atoms/unit volume at a distance r from an i-type atom, averaged over all i-type atoms. The functions $\rho_{ij}(r)$ contain only radial information, all directional information is destroyed by the averaging process.

The purpose of this work is to examine the details of the short range order in Y based metallic glasses. Short range order is taken to mean the arrangement of atoms in the first nearest neighbor shell about a given atom. Our basic tool is the Mössbauer Effect in Fe^{57}. Unlike the diffraction techniques mentioned above, Mössbauer Effect spectroscopy is a truly microscopic probe which is sensitive to both the chemical and topological short range order about the resonant atom. Since Mössbauer's original work in 1957, this technique has been extensively used in both crystalline and amorphous solids. In a Mössbauer Effect (ME) experiment one observes the emission of gamma rays in one solid (the source) and the subsequent resonance absorption of these gamma rays by similar nucleii in another solid (the absorber). The gamma rays result from transitions between two nuclear levels. In fig.1 we show some of the nuclear energy levels of Fe^{57}. The ME transition in this case is from the spin 3/2 to the spin 1/2 levels (E_γ =14.4 keV). The spin 3/2 excited state is indirectly fed by the decay of Co^{57}($t_{\frac{1}{2}}$= 270.5 days). The excited state is metastable which means that there will be an intrinsic spread of γ-ray energies of full width at half maximum Γ given by $\Gamma\tau = h$ where τ is the mean lifetime of the excited state. This width is on the order of 10^{-9} eV and is much smaller than the other processes associated with the emission and absorption of gamma

rays (i.e. recoil energy 10^{-4} eV and thermal broadening 10^{-3} eV). The probability of absorption under normal circumstances is therefore very small. In 1957 Mössbauer[6] found that the 129 keV γ-ray of Ir^{191} could be emitted and absorbed without the loss of energy due to the recoil of the nucleus and without thermal broadening. The probability of recoil free emission or absorption (f) in a harmonic solid is given by $f = \exp(-E_\gamma^2 \langle x^2 \rangle/(hc)^2)$, where $\langle x^2 \rangle$ is the mean square displacement of the atom in the solid. The recoil free radiation has a width Γ and the distribution of energies about E_γ is given by the Breit-Wigner[7] formula. This leads to a Lorentzian shape of the emission and absorption lines.

$$N(E) = \frac{f\Gamma}{2\pi} \quad \frac{dE}{(E-E_\gamma)^2 + (\Gamma/2)^2}$$

where N(E) is the number of transitions /unit energy with energy between $(E_\gamma - E)$ and $(E_\gamma - E + dE)$. The resonant absorption cross-section $\sigma(E)$ can be expressed as

$$\sigma(E) = \frac{\sigma_o(\Gamma/2)^2}{(E-E_\gamma)^2 + (\Gamma/2)^2}$$

where σ_o is the effective nuclear cross section. The decrease in transmission of recoil free gamma rays emitted by the source and passing through the absorber in the thin absorber limit as a function of energy (E) of the incident gamma rays is

$$I(E) = \frac{\Gamma/\pi}{(E-E_\gamma)^2 + \Gamma^2}$$

For finite thickness absorbers I(E) has the same basic shape (Lorentzian) but will appear to be broadened.

The usefulness of the ME comes from the fact that the widths of the emission and absorption processes are comparable in energy to the interactions between the nuclear and electronic systems. These interactions are termed hyperfine interactions[8] and in our discussion below we will describe them for the case of Fe^{57}. There are three principal hyperfine interactions to consider: isomer shift, electric quadrupole, and magnetic dipole.

During the nuclear transition the effective size of the nucleus changes thereby changing the nuclear-electronic interaction. This interaction does not split the nuclear levels, but instead results in a uniform shift of these levels which is proportional to the charge density at the nuclear site ($e|\Psi(0)|^2$). This shift occurs in both the source and absorber which are generally in different chemical environments. In a ME experiment one measures the difference between the energy transitions in the source and the absorber which allows a determination of the isomer shift (IS)

$$IS = C(R_{ex}, R_{gd}, Z) \times (|\Psi_a(0)|^2 - |\Psi_s(0)|^2)$$

where C is a function of the nuclear charge (Z) and the effective radii of the excited (R_{ex}) and ground (R_{gd}) states, and s and a refer to the source and absorber. For a given nucleus the IS is determined solely by the difference in electron density at the nuclear site. This electron density is determined primarily by the s-electrons; however, due to

shielding effects the populations of p, d, and f electrons can also make a contribution. For a given source ($|\Psi_s(0)|^2$-fixed) the IS is given by the electron density in the absorber at the nuclear site. In transition metals, a convenient way to express the differences in IS between chemical environments is by the expression[9]

$$\Delta IS = a\Delta n_d + b\Delta n_c + c\Delta V/V_o$$

where the Δn_d and Δn_c terms represent the changes in the d-electron and conduction electron populations, the $\Delta V/V_o$ term takes into account the changes in the spatial extent of the electronic wavefunctions, and a, b, and c are constants. From this expression we expect the IS to be sensitive to the type and number of nearest neighbors about the resonant atom and to the volume of its site.

The electric quadrupole interaction is the result of the interaction between the quadrupole moment (Q) of the nucleus and the electric field gradient produced by charges external to the nucleus given by the Hamiltonian

$$\mathcal{H}_Q = \frac{e^2qQ}{4I(2I-1)} \{3I_Z^2 - I(I+1) + \eta(I_+^2+I_-^2)/2\}$$

where eq is the z-component of the electric field gradient (EFG), $\eta = \frac{(EFG)_x-(EFG)_y}{(EFG)_z}$, $|EFG_z| > |EFG_x| \geq |EFG_y|$, and I, I_z, I_+, and I_- are the conventional nuclear spin operators. For Fe^{57} (spin $3/2 \rightarrow 1/2$ transition) the ground state is not split and the excited state (I=3/2) is split into two sublevels. The two eigenvalues for a purely quadrupole

interaction are

$$E = \frac{e^2qQ}{4}(1+\eta^2/3)^{\frac{1}{2}}$$

$$E = (-1)\frac{e^2qQ}{4}(1+\eta^2/3)^{\frac{1}{2}}$$

In an experiment we measure the splitting (QS) of the I=3/2 levels.

$$QS = \frac{e^2qQ}{2}(1+\eta^2/3)^{\frac{1}{2}}$$

QS contains information on the local environment of the resonant atom via the atomic parameters eq and η .

$$eq = -\int \frac{\rho_e(r)(3Z^2-r^2)}{r^5} d^3r$$

$$\eta = -3\int \frac{\rho_e(r)(x^2-y^2)}{r^5} d^3r$$

where $\rho_e(r)$ is the charge density distribution outside of the nucleus producing the EFG. The contributions to $\rho_e(r)$ are usually divided into two groups. The first is the contribution due to non-spherically symmetric (p, d, and f) valence electrons localized on the resonant atom. The second contribution is due to charges localized on the neighboring ions in the solid. Due to the short range $(1/r^3)$ of eq and η the most important contributions will come from the first and second nearest

neighbors. In fig. 1 we show the effects of the IS and QS interactions on the nuclear levels of a spin 3/2 → 1/2 transition (appropriate for Fe^{57}). In the absence of an EFG ($e^2qQ=0$) the levels are simply shifted by the IS interaction. With a non-zero EFG ($e^2qQ\neq0$) some of the degeneracy of the 3/2 level is lifted and the level is split into two sub-levels. In Fe^{57} the nuclear transition is M1(magnetic dipole, $\Delta m=0, \pm1$) so that transitions from both these sub-levels are permitted. It is important to note that the centroid of the two sub-levels is independent of e^2qQ so that both the IS and QS can be deduced from the experiments.

The final hyperfine interaction to be considered is the magnetic dipole interaction. This is the interaction between the magnetic moment of the nucleus and the magnetic field at the nuclear site. It is important when the material diplays some sort of magnetic ordering (ferromagnetism, antiferromagnetism, etc.). The Hamiltonian for the magnetic dipole interaction is

$$\mathcal{H}_M = -g\mu_N I_Z H$$

where g is the nuclear g-factor and μ is the nuclear magneton. In the absence of an electric quadrupole interaction the resulting energy eigenvalues are

$$E(m) = -g\mu_N Hm \qquad (m = I, I-1, \ldots -I)$$

All the degeneracy of the nuclear levels is removed and for the case of Fe^{57} the excited state level splits into 4 sub-levels and the ground state level is split into 2 sub-levels (6 possible transitions).

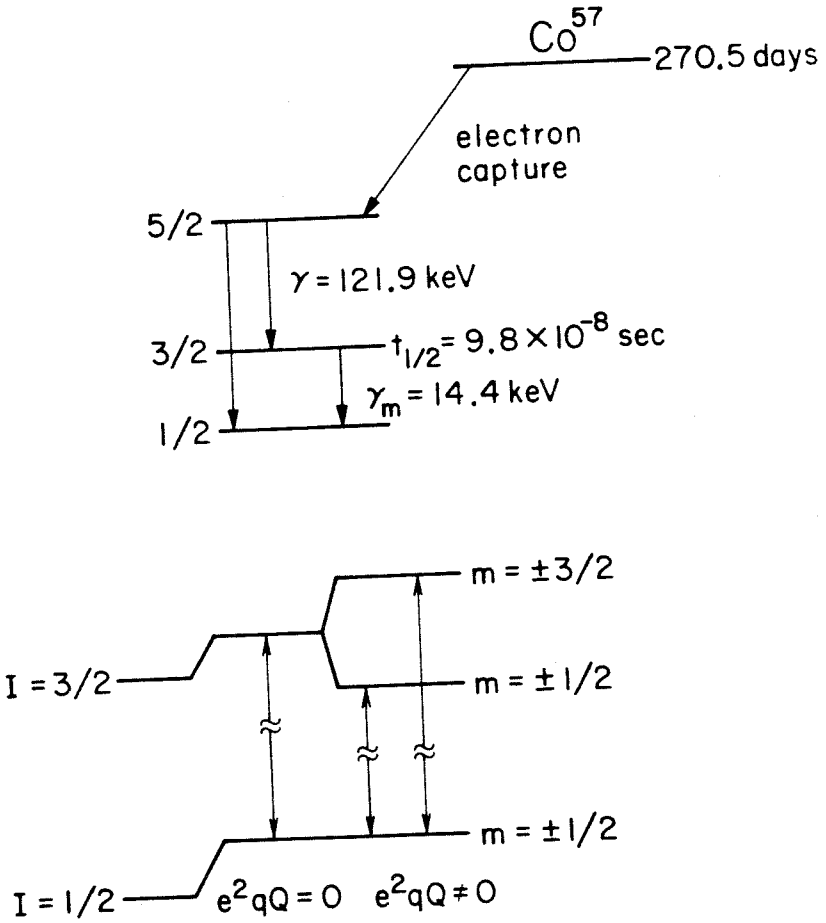

Fig. 1 (Top) Decay of $Co^{57} \rightarrow Fe^{57}$ showing the first three excited states of Fe^{57}. γ_m is the ME γ-ray. (Bottom) Effect of pure IS ($e^2qQ = 0$) and combined IS and QS intereactions on a spin $3/2 \rightarrow 1/2$ transition.

In our discussion above we have treated the three hyperfine interactions independent of each other. This is correct for the IS since its effect is to change the energy of all the levels. However, the electric quadrupole and magnetic dipole interactions cannot be treated separately and the level splitting must be found by diagonalizing the total Hamiltonian

$$\mathcal{H} = \mathcal{H}_Q(I_Z') + \mathcal{H}_M(I_Z)$$

where I_z' and I_z are defined with respect to two different coordinate systems. In the most general case I_z is not a good quantum number and the eigenstates are linear combinations of states having different values of I_z. A description of the ME spectrum in this case requires the determination of H, eq, η, and five angles relating I_z, I_z', and the EFG tensor to a common axis. A simple example of a combined electric quadrupole-magnetic dipole interaction we will encounter later is the case of an axially symmetric EFG tensor with its symmetry axis at an angle Θ with respect to the magnetic axis. For $e^2qQ/\mu H << 1$ and I=3/2 the eigenvalues are

$$E(m) = -g\mu_N Hm + (-1)^{|m|+\frac{1}{2}} (e^2qQ)(3\cos^2\Theta-1)/8$$

The majority of the ME work on metallic glasses has been on magnetic materials. These studies have concentrated on the metal-metalloid glasses such as Fe-B. Some of these materials are being considered for use in magnetic devices and the ME has served as a

useful probe of the magnetic properties of these materials. In fig. 2 we show the ME spectrum of one of the first ferromagnetic metallic glasses prepared from ref. 10. Below its Curie temperature, all three hyperfine interactions will have an influence on the spectrum. This fact makes the analysis of the ME data difficult and frequently ambiguous. In our work we have concentrated on nonmagnetic metallic glasses. There have been no systematic ME studies on such materials. A few studies have been made in which Fe was added to various isolated nonmagnetic metallic glasses (Cu-Zr[11], Nb-Ni[12], and Pd-Si[13]). The situation is quite different with regards to amorphous semiconductors where systematic ME studies have been performed on a number of binary alloys (Ge-Te[14], Se-Te[15,16], and As-Te[17,18]). In fig. 3 we show the I^{129} ME spectra for two As-Te glasses from ref. 18. The ME transition in I^{129} is from a spin 5/2 to a spin 7/2 level and the electric quadrupole splitting involves 12 resonance lines. The positions and relative intensities of these lines are determined by the IS and the two EFG parameters. The middle spectrum in fig. 3 shows that a simple average Te site is a poor representation of the $As_{30}Te_{70}$ sample. A much better fit to this spectrum and to the spectrum of the $As_{50}Te_{50}$ sample is obtained by assuming two distinct Te sites. The second Te site is shown in the top spectrum of fig. 3 and has been identified as a threefold coordinated Te site. The analysis shows that the relative amount of threefold Te sites increases with increasing Te content. This information can be used to explain many of the properties of these glasses such as the compositional variation of

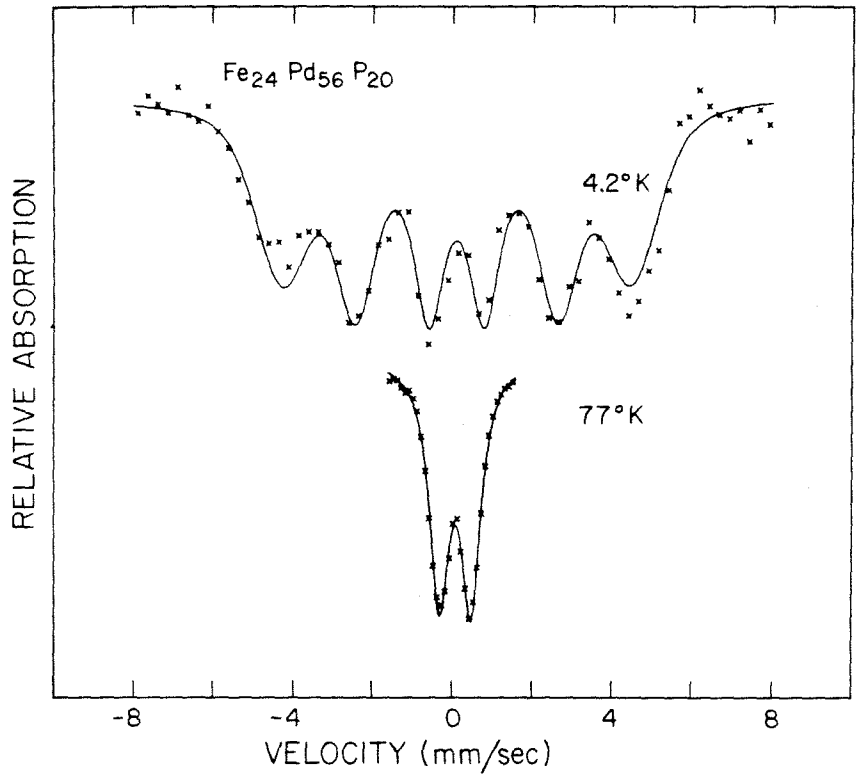

Fig. 2 ME spectra of the glass $Fe_{24}Pd_{56}P_{20}$ taken above (77 K) and below its Curie temperature (4.2 K).

density, microhardness, and electrical conductivity.[18]

The metallic glass system we have chosen to study is the Y-Fe system. Fe is the smallest atom in which ME experiments can be performed and which forms metallic glasses. Y, on the other hand, is one of the largest atoms which form glasses. The equilibrium phase diagram of this system is simple and as we will see, it contains a chemically ordered compound (YFe_2). It was anticipated that this fact along with the size difference between Y and Fe would lead to some chemical ordering in Y-Fe glasses. Except for the lack of magnetic interactions, the Y-Fe system serves as the prototype of the rare earth- transition metal glasses.

It was also the purpose of this study to try to learn something about the crystallization of metallic glasses. The usual techniques for the study of crystallization are differential scanning calorimetry (DSC), X-ray diffraction, and electron microscopy. These techniques tend to concentrate on the macroscopic nature of the process. The emphasis is on the crystallization temperature and identifying the resulting crystalline phases. The ME can provide information on the microscopic changes occurring during crystallization. The only ME work on this subject has been on glasses such as Fe-B. The crystalline compounds which form in these materials are very complicated and the analysis of the ME spectra is difficult. For example, fitting some of the ME spectra of partially crystalline $Fe_{80}B_{20}$ samples required 30 lines and 34 independent parameters. In the Y-Fe glasses we will study, the glasses transform into two crystalline phases. Only one of these

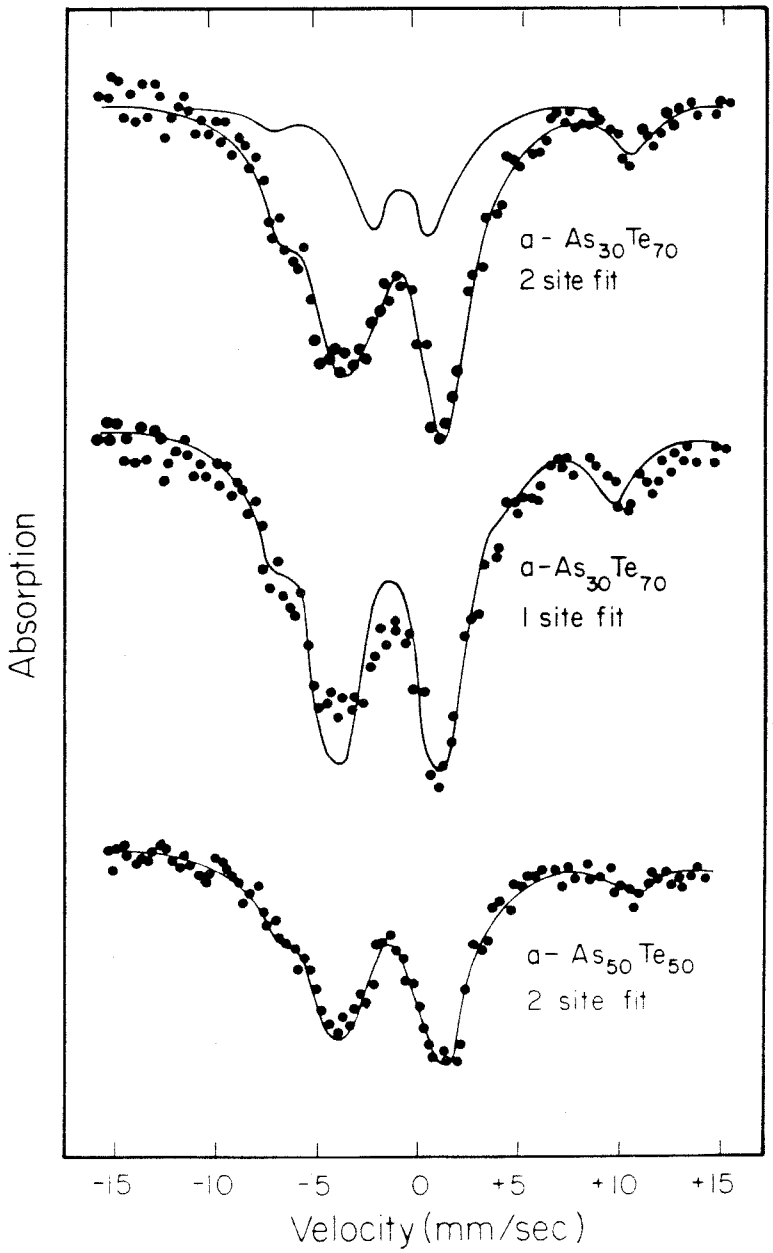

Fig. 3 I^{129} ME spectra of liquid quenched As-Te glasses, taken at 4.2 K.

phases contains Fe. This Fe containing crystalline phase has a ME which is very different from that of a glassy sample. This difference allows us to study the changes in the glassy phase upon crystallization.

II. EXPERIMENTAL PROCEDURES

Alloys were prepared by induction melting of the appropriate constituents in a water cooled Ag boat. The starting materials were at least 99.9% pure and the typical size of an ingot was 2 grams. The weight loss after alloying was typically less than 0.05% and the compositions reported are the nominal ones. The following binary and ternary alloys were prepared: $Y_{1-x}Fe_x$, $Y_{66}(Fe_yTM_{1-y})_{34}$(TM= Mn, Fe, Co, Ni, Cu, and Zn), and $Y(Fe_{0.05}TM_{0.95})_2$(TM= Mn, Fe, Co, and Ni). Rapidly quenched samples of some of these materials were prepared by the piston and anvil technique described in detail in ref. 19. The procedure was to load approximately 30 mgs. of the material in a narrow quartz tube and to melt it in the presence of a flowing He atmosphere. When the sample had melted it was ejected from the quartz at which point it activates a solenoid releasing a piston. The rapidly moving piston smashes the sample against the anvil. The surfaces of both the piston and anvil are made of a Cu-Be alloy which has been specially heat treated for maximum hardness and thermal conductivity. The quenching rate for this technique has been estimated to be on the order of 10^6 degrees/sec. Samples prepared this way were in the form of foils approximately 30 μm thick.

The disposition of the as-quenched samples was determined by X-ray diffraction experiments using Cu K_α and Mo K_α radiations. The scanning rate for a typical diffraction experiment was 0.05°/min. Foils whose diffraction pattern consisted of a smooth featureless band and no sharp Bragg reflections were classified as amorphous.

Density measurements were made on a number of the foils using a microbalance and a toluene bath. The weight of the foil was measured in air and a toluene bath from which we deduce the density. A typical foil used for these measurements weighed 30 mgs. Somewhere between 3 and 7 foils of each composition were measured. The error in the density measurements was less than 0.5%.

A series of experiments was undertaken to study the crystallization of some of these materials. One of the most widely used techniques is DSC. In these measurements the temperature of the sample is increased at a uniform rate and the heat evolved during various transformations is recorded. We used a commercially available unit (Perkins-Elmer DSC-I) and a scanning rate of 10 K/min. The typical size of the sample was 7 mgs. Similar information can be obtained by measurements of the resistivity of the foils at high temperature. In these experiments the sample is mounted in a high temperature furnace in a flowing He atmosphere. The resistence of the sample is measured using a standard four point probe and the temperature is monitored by a Pt-Pt(Rh) thermocouple. The rate of temperature increase for these measurements was on the order of 1 K/min.

The primary experimental tool of this study is ME spectroscopy using the resonance in Fe^{57}. A schematic of the experimental setup is shown in fig.4. The source is mounted on an electromechanical transducer which is synchronized with a time base multichannel analyser (MCA). The source is moved in a constant acceleration mode which means that the time base of the MCA is a linear velocity scale. The photons leaving the source and passing through the absorber are detected

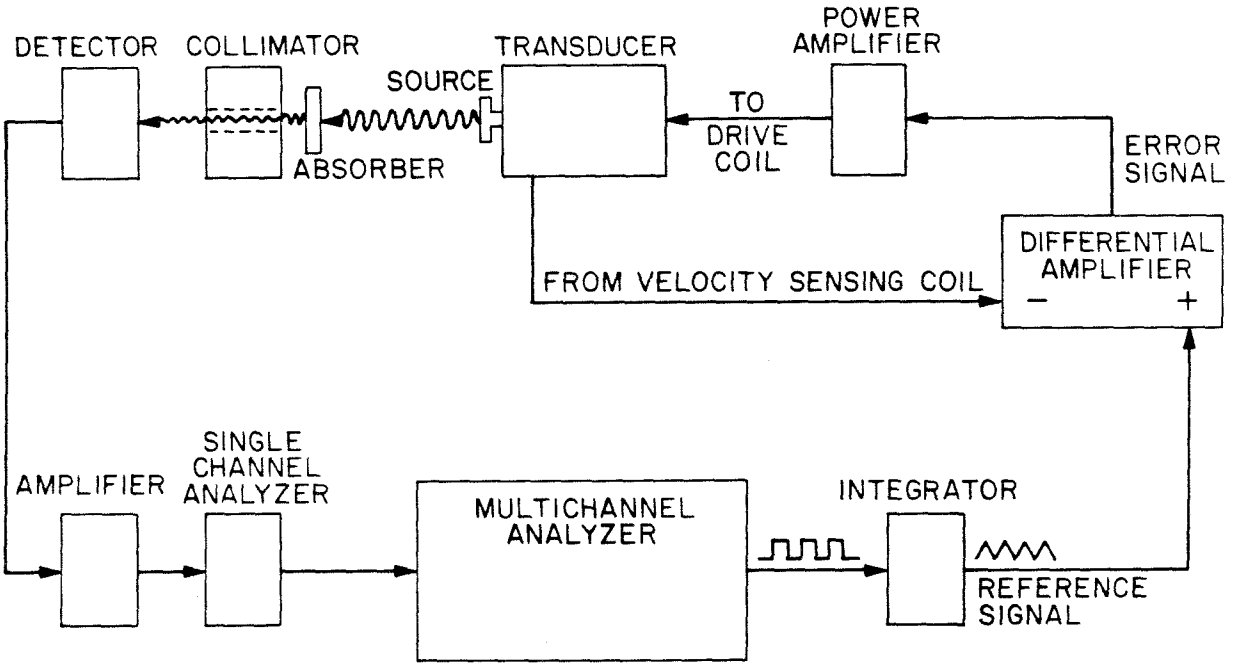

Fig. 4 Experimental setup for ME experiments.

by a $Kr(CO_2)$ proportional counter. The signals from the proportional counter are fed into a spectroscopic amplifier and an energy window is set by the single channel analyser (SCA). The output of the SCA is then sent to the MCA. The object of this apparatus is to record the number of photons in a preset energy range which pass through the stationary absorber as a function of the velocity of the source.

The source used for our experiments is Co^{57} in a Rh host. As shown in fig. 1, the decay of Co^{57} populates the excited states of Fe^{57}. The $3/2 \rightarrow 1/2$ transition in Fe^{57} produces the Mössbauer gamma ray (14.4 keV). In the top curve of fig. 5 we show the output of the spectroscopic amplifier (pulse height analysis) for our Co^{57}(Rh) source. The efficiency of the $Kr(CO_2)$ proportional counter decreases very rapidly beyond about 30 keV so that the higher energy photons (121.9 and 136.3 keV) are not directly detected. The Kr $K_{abs.\ edge}$ is at 14.32 keV so that we get an anomalously high efficiency for the 14.4 keV Fe^{57} gamma rays. In the $3/2 \rightarrow 1/2$ transition of Fe^{57}, only a fraction of the time ($\sim$9%) does it result in the emission of a gamma ray. A competing process is internal conversion in which the energy of the transition is used to photoionize the 1s electron of Fe. This leaves holes in the K shell which are annihilated by transitions from higher lying electrons accompanied by the emission of Fe K X-rays (6.5 keV). In addition to these photons, we also see a weak contribution from Rh K X-rays which are produced by the photoionization of Rh 1s electrons by the higher energy gamma rays. In the lower curve of fig. 5 we see the pulse height analysis of the radiation passing through a Y-Fe absorber from the Co^{57}(Rh) source.

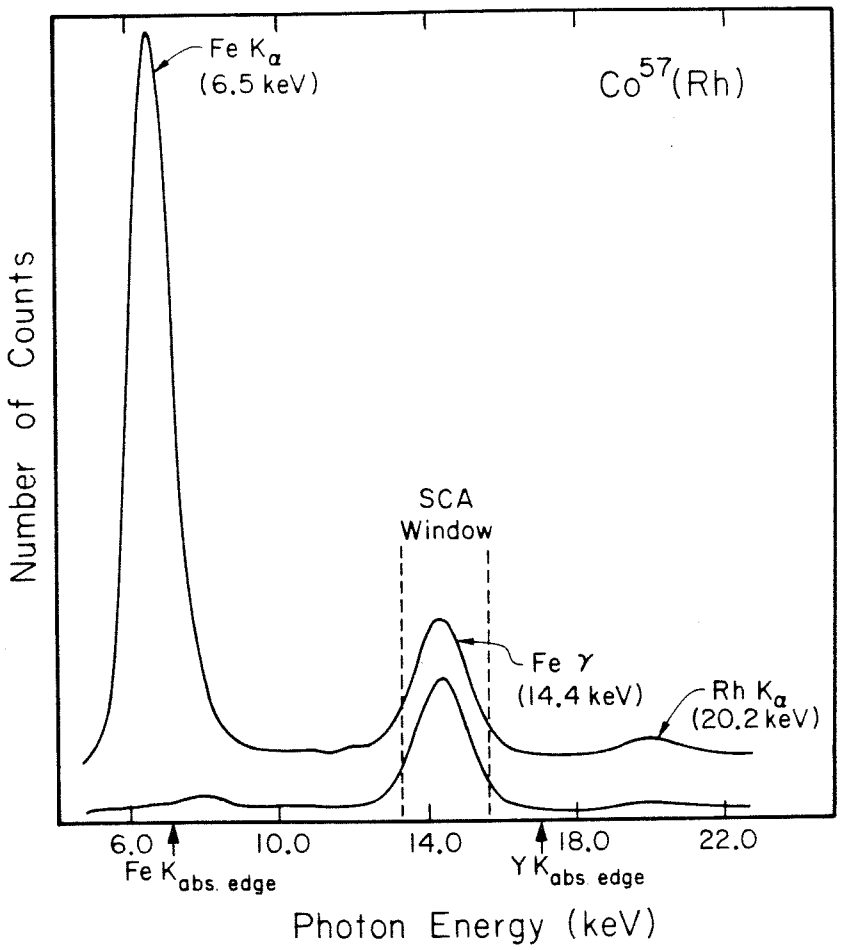

Fig. 5 PHA spectra of Co^{57} (Rh) source taken with a $Kr(CO_2)$ proportional counter. The top curve is just the Co^{57} (Rh) source and the bottom curve is with a Y-Fe absorber between the source and detector.

Because of the locations of the Fe $K_{abs.\ edge}$ and the Y $K_{abs.\ edge}$, the Y-Fe absorber nicely filters out most of the unwanted radiation from the source. The position and width of the SCA energy window is also illustrated in fig. 5. The Co^{57} atoms in the source are in a cubic environment (Rh is fcc) and therefore the radiation emitted from the source has an energy distribution which is Lorentzian having its center at about 14.4 keV and a width of about 5×10^{-10} ev. This corresponds to the case $e^2qQ = 0$ in the bottom of fig. 1. The energy of the nearly monoenergetic gamma rays coming from the source is modulated by Doppler shifting (by a velocity v) the source. The Doppler shift results in an energy shift of the photons by an amount $\Delta E = (v/c)E_\gamma$. The velocities used in the experiments are on the order of 1 mm/sec which corresponds to an energy shift of about 4.8×10^{-9} eV.

Returning to fig. 4 we see that the MCA records the number of transmitted photons passing through the absorber as a function of the incident photon energy. Resonance absorption of the incident photons will occur when the nuclear levels of the Fe atoms in the absorber coincide with the energy of the photons emitted from the source. In fig. 6 we show the ME spectrum of Fe^{57} atoms in the crystalline compound $Y(Co_{0.95}Fe_{0.05})_2$. In this compound the Fe atoms are all crystallographically equivalent and experience a single unique value of an electric field gradient (eq). We illustrated the quadrupole splitting of the Fe^{57} levels for this case in fig. 1. The spacing of the lines in the spectrum of fig.6 directly gives the energy splitting (QS) of the I = 3/2 levels. The QS of Fe in this sample corresponds to an

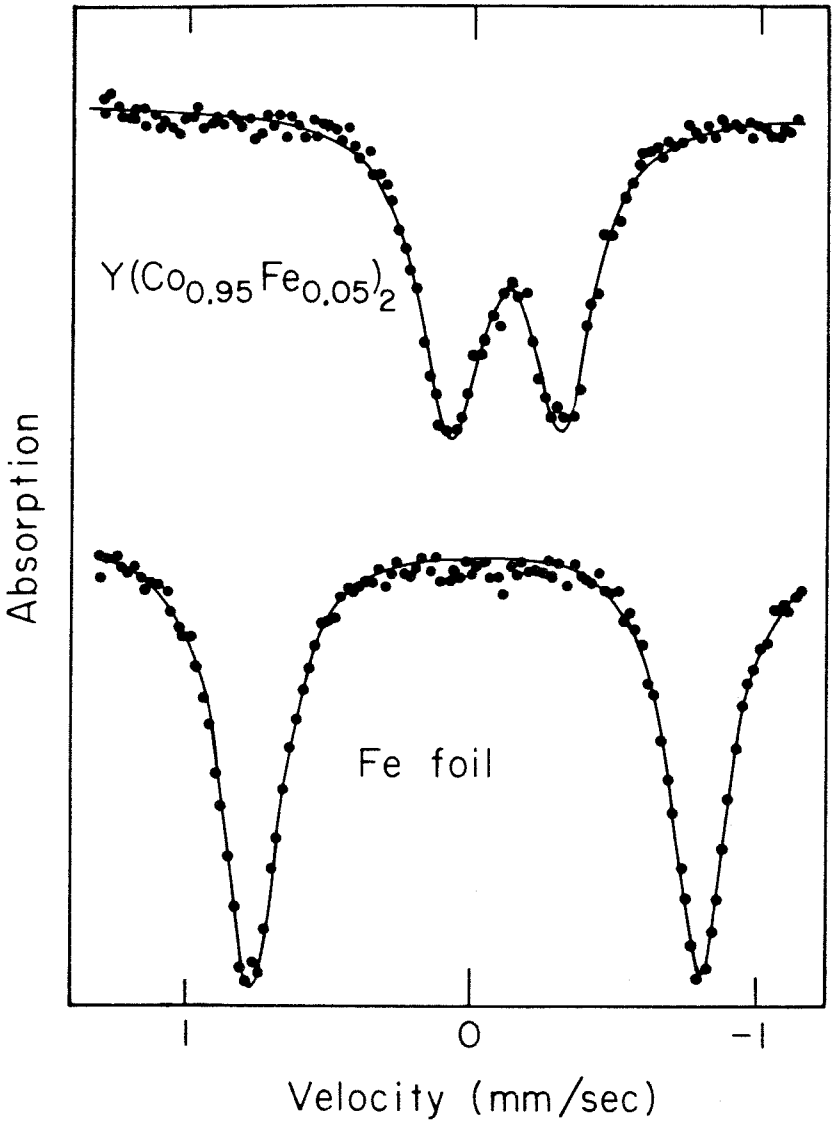

Fig. 6 ME spectra taken at room temperature. The dots are the experimental data points and the solid lines are the results of fitting the spectra to a pair of Lorentzian lines.

energy difference of 2.2×10^{-9} eV. If the absorber contains n different Fe sites then the ME spectrum (for the nonmagnetic case) will be a superposition of 2n Lorentzian lines. Each of these n sites is characterized by its value of IS , QS, and intensity. The number of Fe atoms associated with a given site is proportional to its contribution to the area under resonance in the spectrum divided by its recoil free fraction.

The majority of the ME experiments were performed at room temperature using a fixed well collimated geometry. The ME drive was calibrated using the splitting of the magnetic hyperfine structure of Fe^{57} in metallic Fe. A typical calibration spectrum is shown in fig. 6. The absorbers were prepared by finely crushing the as-quenched foils, mixing the powder with a MgO filler, and sealing the powder in a lucite holder. The nuclear thickness (t) of Fe^{57} in the powder samples was 0.06 mgs./cm^2. All powder samples were prepared from the powder of a single foil, the powders from different foils were never mixed. To our knowledge, this is the first ME experiments on metallic glasses in which the absorber thickness was kept constant. Because of saturation effects due to the thickness dependence of the resonant absorption cross section the shapes of the absorption lines will change with absorber thickness.[20] A meaningful comparison of different samples can only be made on samples of the same thickness. Exceptions to this procedure of absorber preparation were made for those samples which had less than 2 at% Fe. For these samples the small amount of Fe^{57} did not permit the fabrication of t = 0.06 mgs./cm^2 absorbers from a single foil and the as-quenched foils were directly used as absorbers.

A series of ME experiments were performed to study the crystallization of Y-Fe metallic glasses. Most of these ME measurements were made using a special high temperature, high vacuum furnace. In this setup the samples in the form of foils are mounted inside of a hollow Cu cylinder on which a heater is wound. This cylinder is suspended from a vacuum can in which are mounted two water cooled mylar windows to permit transmission of the gamma rays. The source, ME drive, and detector are outside the vacuum chamber and were kept at room temperature. The temperature of the sample was monitored by a Pt-Pt(Rh) thermocouple and could be changed from room temperature to 700 K in less than 15 minutes. The long time stability (on the order of 12 hours) of the sample temperature was better than 3 K. The procedure was to mount an as-quenched foil in the furnace, take a ME spectrum, anneal the sample, and take a ME spectrum after the sample returns to room temperature. The advantage of this system is that the sample stays in a fixed geometry during all the heat treatments. For the very long (more than 24 hours) or very short (less than 1 hour) annealing treatments the samples were sealed in evacuated pyrex tubes and heat treated in a separate furnace. Two types of annealing studies were made. In the first type we fixed the time of annealing and varied the annealing temperature (T_A). In the second type, we varied the time of annealing for several fixed values of T_A.

III. EXPERIMENTAL RESULTS

A. $Y_{1-x}Fe_x$ Glasses

From the X-ray diffraction measurements, completely amorphous foils were obtained by rapid quenching from $0.25 \leq x \leq 0.45$. For $x < 0.25$ the foils were not completely amorphous and the Bragg reflections of hcp Y were seen in the patterns. For $x > 0.45$ the as-quenched samples contained traces of hcp Y, YFe_2, and an amorphous phase. In fig. 7 we show the X-ray patterns (using Cu K_α) of several quenched samples and for reference pure Y metal. The $Y_{0.66}Fe_{0.34}$ pattern consists of a smooth featureless band characteristic of metallic glasses. For the $Y_{0.75}Fe_{0.25}$ and $Y_{0.90}Fe_{0.10}$ samples we see the reflections of hcp Y, but no Bragg peaks associated with an Fe containing compound. The nature of these samples is especially interesting and will be discussed in more detail later.

In fig. 8 we show the equilibrium phase diagram of the Y-Fe system and the results of rapidly quenching various compositions. As judged by the success rate in obtaining completely amorphous foils, the glass forming ability is greatest near the eutectic composition. We see in fig. 8 that the glass forming region is centered about the eutectic composition. The results of the density measurements are shown in fig. 9. The compositional variation of atomic density displays an interesting s-like behavior. There is an inflection point near x=0.36 with the curve having a positive curvature for small x and

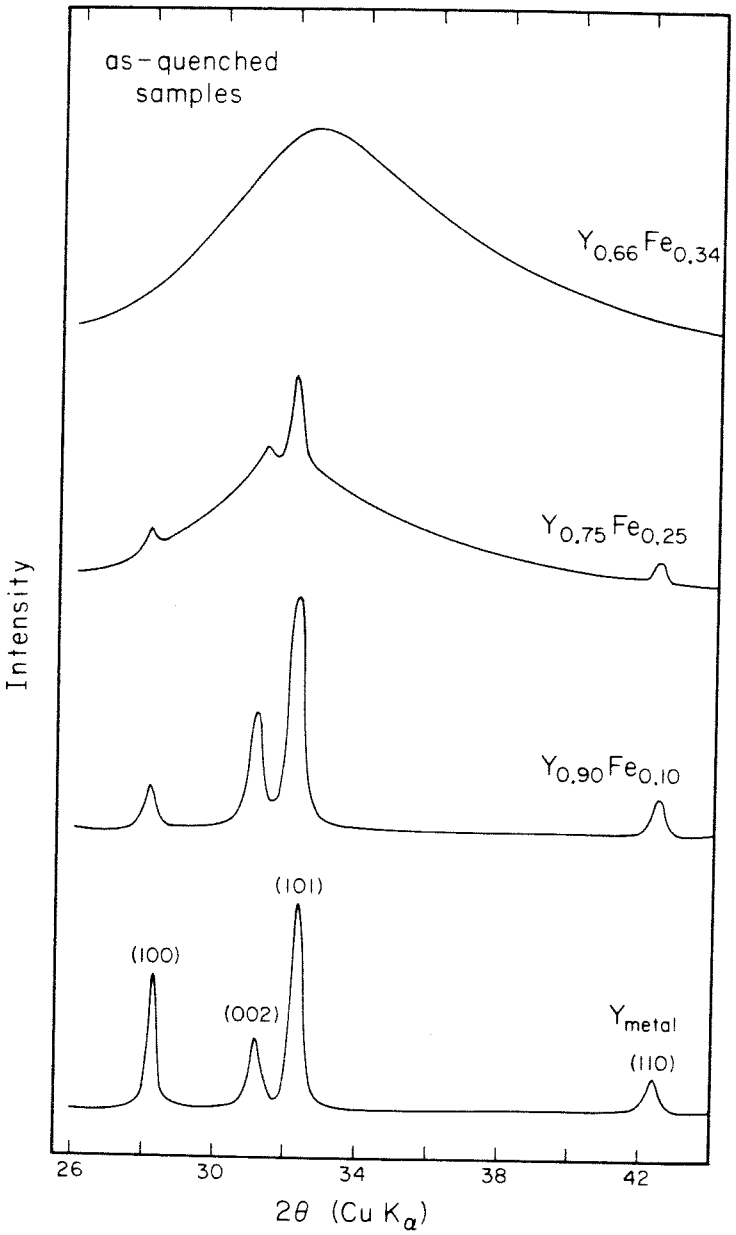

Fig. 7 X-ray diffraction patterns of several as-quenched Y-Fe samples and pure Y metal.

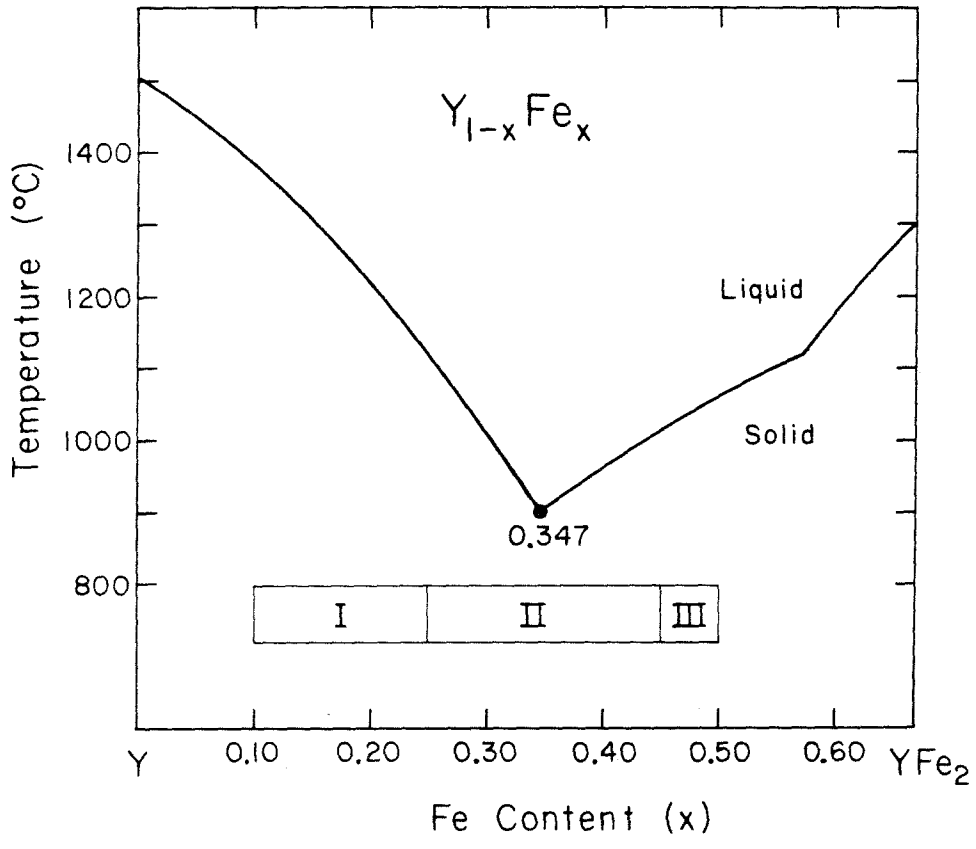

Fig. 8 Equilibrium phase diagram of the binary Y-Fe system. The regions I, II, and III are the results of rapidly quenching various compositions. I stands for hcp Y and an amorphous phase, II for completely amorphous, and III for C-15 and an amorphous phase. The two equilibrium phases are hcp Y and C-15 YFe_2.

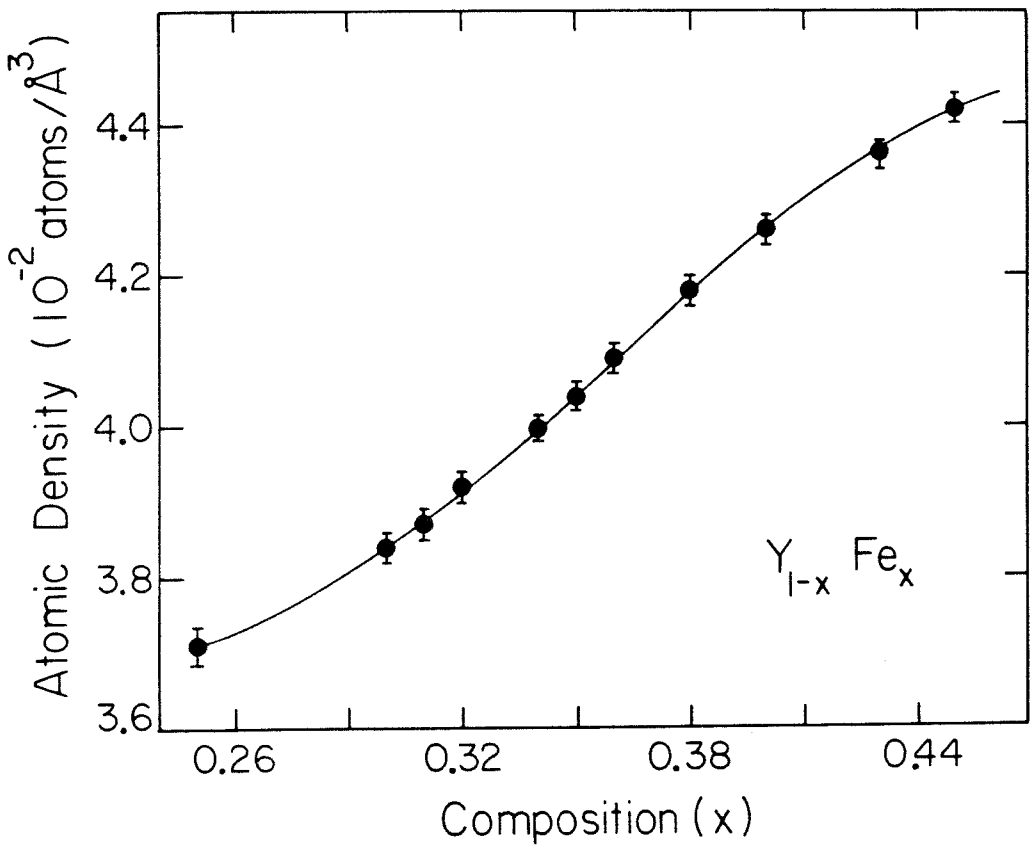

Fig. 9 Atomic density of $Y_{1-x}Fe_x$ glasses as a function of composition.

a negative curvature for large x. Such behavior has not been reported before for a metallic glass system. Our observation is perhaps the result of the fact that both components make a significant contribution to the density of the glass.

The ME spectra taken at room temperature consisted of a pair of reasonably symmetric peaks for all samples studied. This is in contrast to other Fe^{57} ME work on nonmagnetic glasses (Zr-Cu[11], Pd-Si-Fe[13]) in which asymmetric spectra were observed. We show a typical spectrum of a $Y_{0.65}Fe_{0.35}$ sample in fig. 10. The spectrum has been least squares fitted to two slightly broadened Lorentzian lines having equal linewidth from which we extract values of QS and IS. Although a simple two line fit is not bad, there exists some misfit. It is especially noticeable in the region of maximum resonance and near the baseline. This misfit means that the lines are not truly Lorentzian. This coupled with the somewhat broad linewidth (0.35 mm/sec) compared to that of a single phase crystalline material (0.24 mm/sec) means that there is at least a distribution of either QS or IS. In an amorphous material, due to the large amount of chemical and topological disorder one expects both a QS and IS distribution. In fig. 11 we show the results of fitting the $Y_{1-x}Fe_x$ glasses to two Lorentzians. Both the QS and IS values display an interesting step-like variation as a function of composition. The changes we see in these parameters occur near the eutectic composition of the equilibrium diagram. ME spectra of partially crystalline samples were also taken. For x=0.45 the crystalline phase in addition to the amorphous material is YFe_2. The presence of YFe_2 tends to increase the average QS. For x=0.25, a trace of hcp Y was found in some

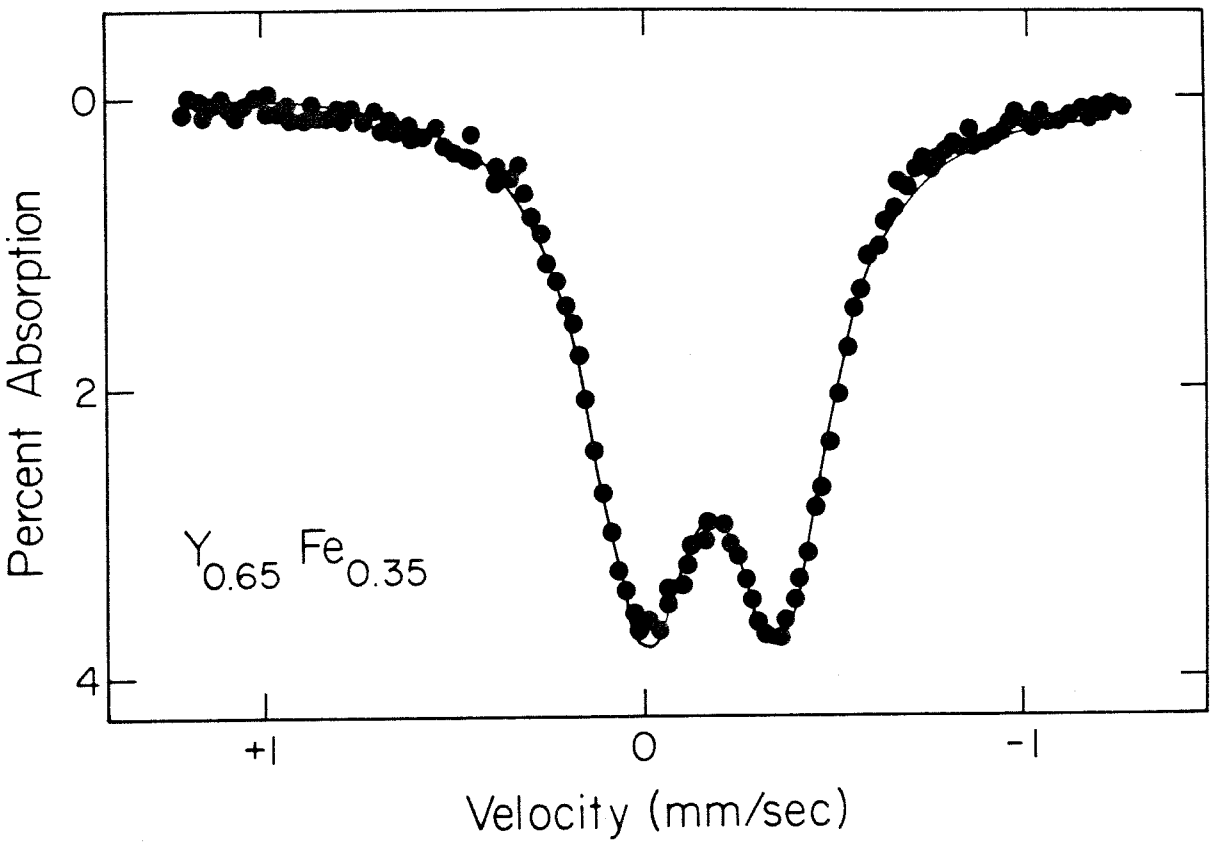

Fig. 10 ME spectrum of $Y_{0.65}Fe_{0.35}$ at room temperature. The smooth line is the result of least squares fitting the spectrum to two Lorentzian lines. The zero of velocity is with respect to α-Fe.

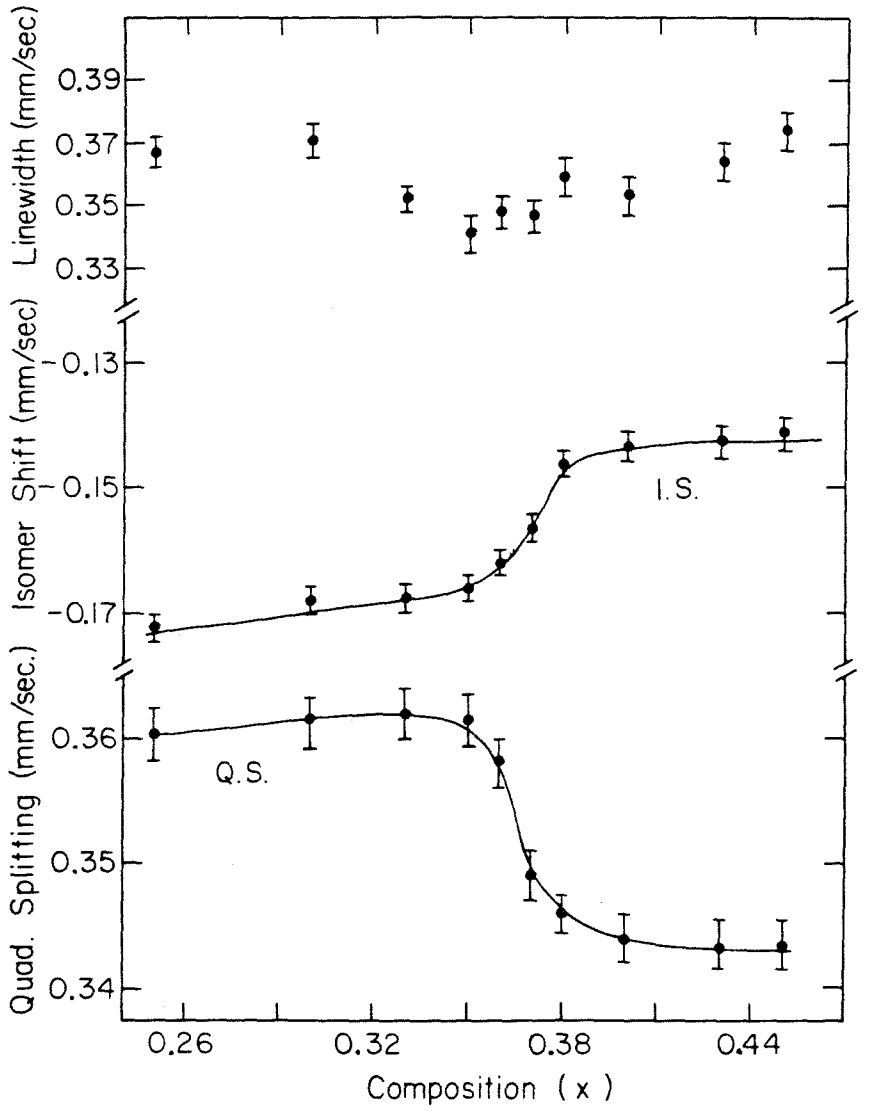

Fig. 11 The compositional dependence of linewidth, IS, and QS for $Y_{1-x}Fe_x$ metallic glasses. The smooth lines have been added to aid in visualizing the data.

of the samples which tended to decrease the average QS. At both ends of the composition range, we see that having a small amount of crystalline material moves the average QS opposite to the direction of the jump. We conclude from this that the changes in QS and IS are intrinsic to the amorphous materials and are not the result of crystalline inclusions in the samples. The Γ values, which are a measure of the uniqueness of the Fe environments, display a broad minimum near the middle of the glass forming region (fig. 11). Although the extreme compositions were found to be amorphous by X-ray diffraction experiments, it is possible that they contain some sub-critical crystalline nucleii. The Fe atoms in these nucleii are likely to have a different IS or QS than the amorphous material and their presence will broaden the observed linewidth.

B. $Y_{66}(Fe_yTM_{1-y})_{34}$ Glasses

We found that metallic glasses could be produced by rapid quenching for all alloys of the form $Y_{66}(Fe_yTM_{1-y})_{34}$(TM = Mn, Fe, Co, Ni, Cu, and Zn). ME spectra of a variety of compositions are shown in figs. 12, 13, and 14. For y=1.00 ($Y_{66}Fe_{34}$) we see that the the spectrum consists of two symmetric peaks. The addition of Mn (fig. 12) causes the spectra to progressively lean to the left (left asymmetric). Conversely, the addition of Co results in the spectra becoming right asymmetric (fig. 13). The addition of Ni and Cu leave the spectra reasonably symmetric while the addition of Zn results in the spectra again becoming left asymmetric (fig. 14). In fig. 15 we show that as an approximation the $Y_{66}Fe_{34}$ spectrum can be fit as the sum of two broad

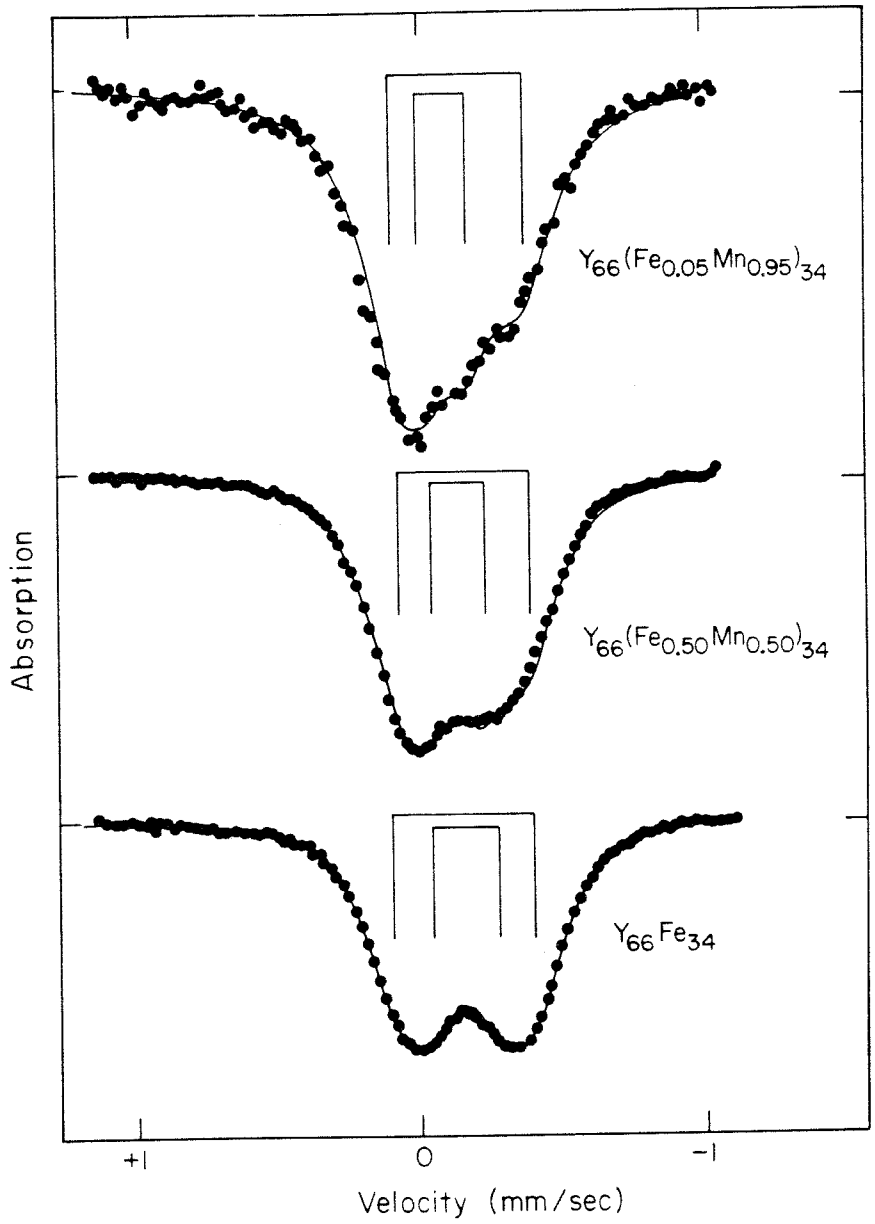

Fig. 12 Room temperature ME spectra of $Y_{66}(Fe_yMn_{1-y})_{34}$ metallic glasses. The solid lines passing through the data points represent the least squares fits of the spectra to two pairs of lines. The peak positions and intensities are shown above the data by the vertical bars.

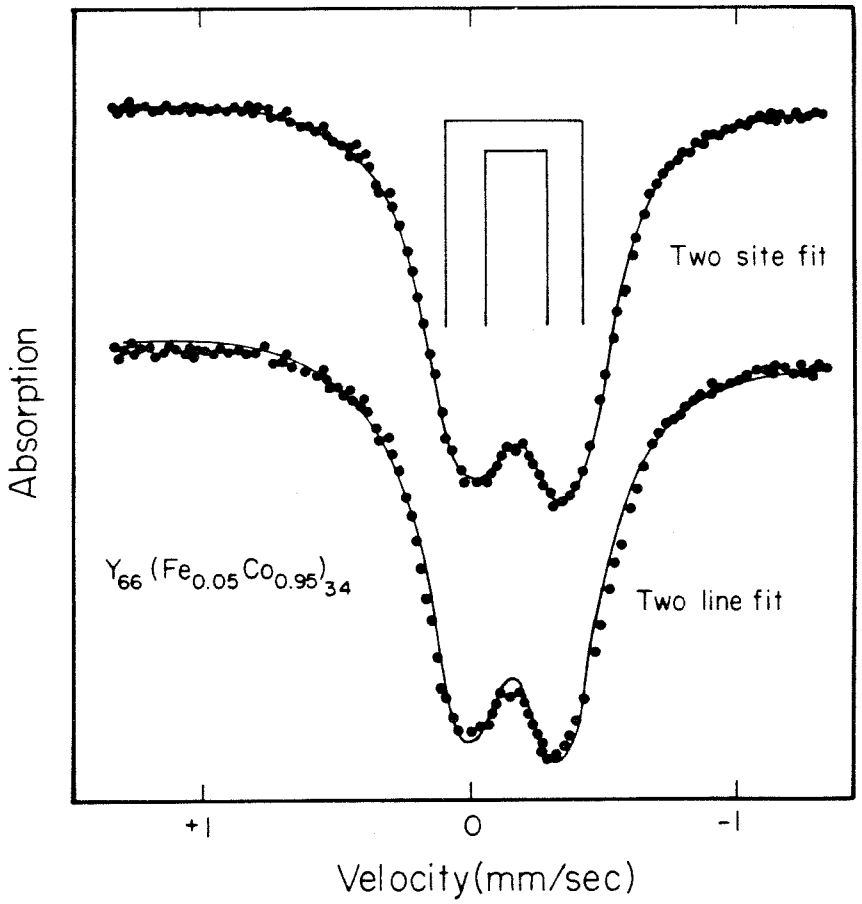

Fig. 13 ME spectrum of $Y_{66}(Fe_{0.05}Co_{0.95})_{34}$ glass fitted to two sites (top) and to two asymmetric lines (bottom).

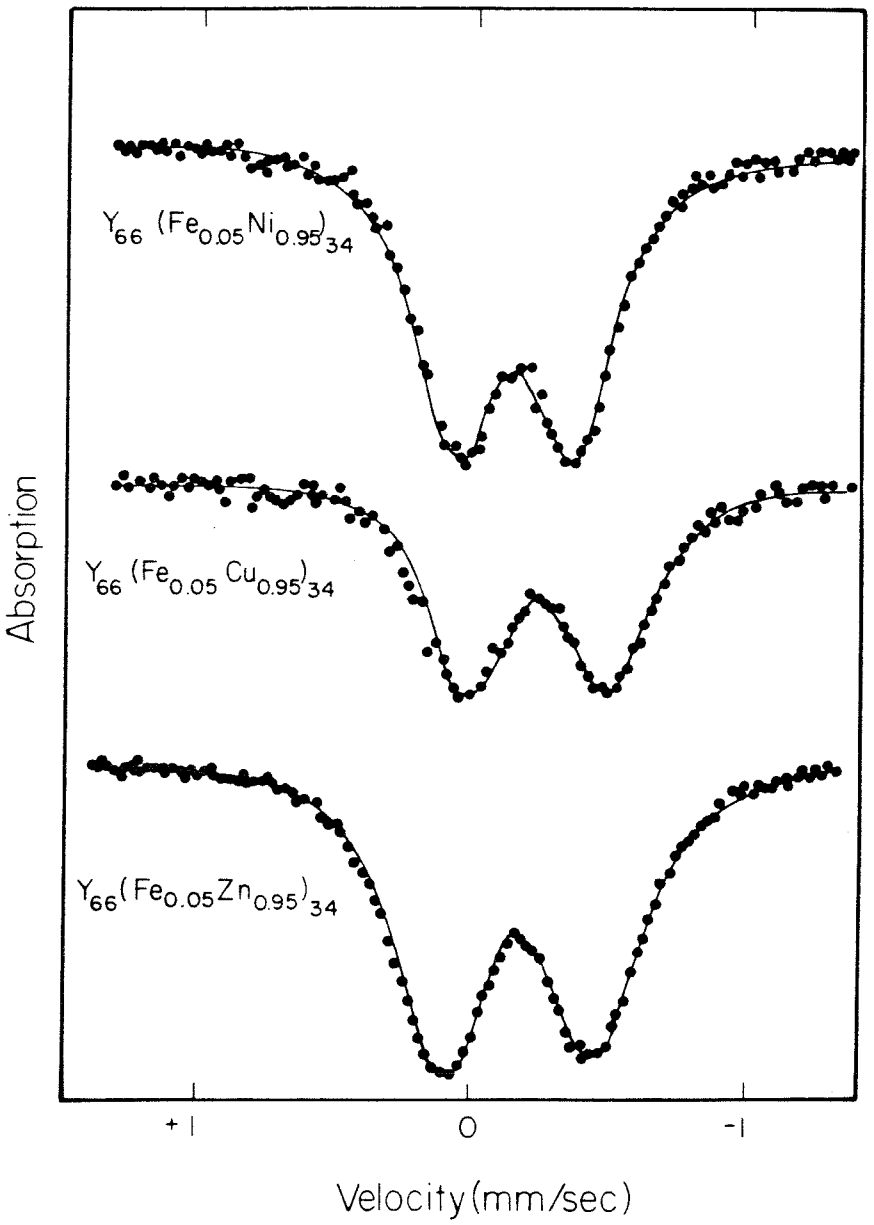

Fig. 14 ME spectra of $Y_{66}(Fe_{0.05}TM_{0.95})_{34}$ (TM = Ni, Cu, and Zn) metallic glasses fitted to two Fe sites.

Lorentzian lines (one site fit). In fig. 12 we show the same $Y_{66}Fe_{34}$ spectrum fitted to a model which assumes two Fe sites and we see that it is visibly better representation of the spectrum than the one site fit. The spectra having higher Mn content cannot be reasonably fit to two broad Lorentzian lines; a minimum of a least two doublets is required to understand the data. There are two important properties of these two site fits. First, the widths of the lines found from these fits are only slightly larger than those usually observed for crystalline materials. Second, we were able to consistently fit the spectra of the metallic glasses $Y_{66}(Fe_yMn_{1-y})_{34}$ for all values of y (see fig. 12). In fig. 13 we compare the two site fit of the $Y_{66}(Fe_{0.05}Co_{0.95})_{34}$ spectrum to a two line (single site) fit, allowing the two lines to have unequal intensities. It is clear that the two site model is a better representation of the spectrum; this is true for all members of the Co system. For TM = Ni and Cu, the situation is not as clear since the spectra are once again symmetric. Because the TM = Zn spectrum is asymmetric, the two site fit once again looks better than a two line,single site fit. It is important to keep in mind here that this method of fitting is only approximate and that one should properly be talking about fitting distributions of Fe sites. However, we find that the two site model gives an adequate representation of the data, and furthermore provides a useful framework for describing its implications.

The results of fitting the spectra to two Fe sites are shown in figs. 12, 13, and 14 and are listed in tables I and II. Each site is

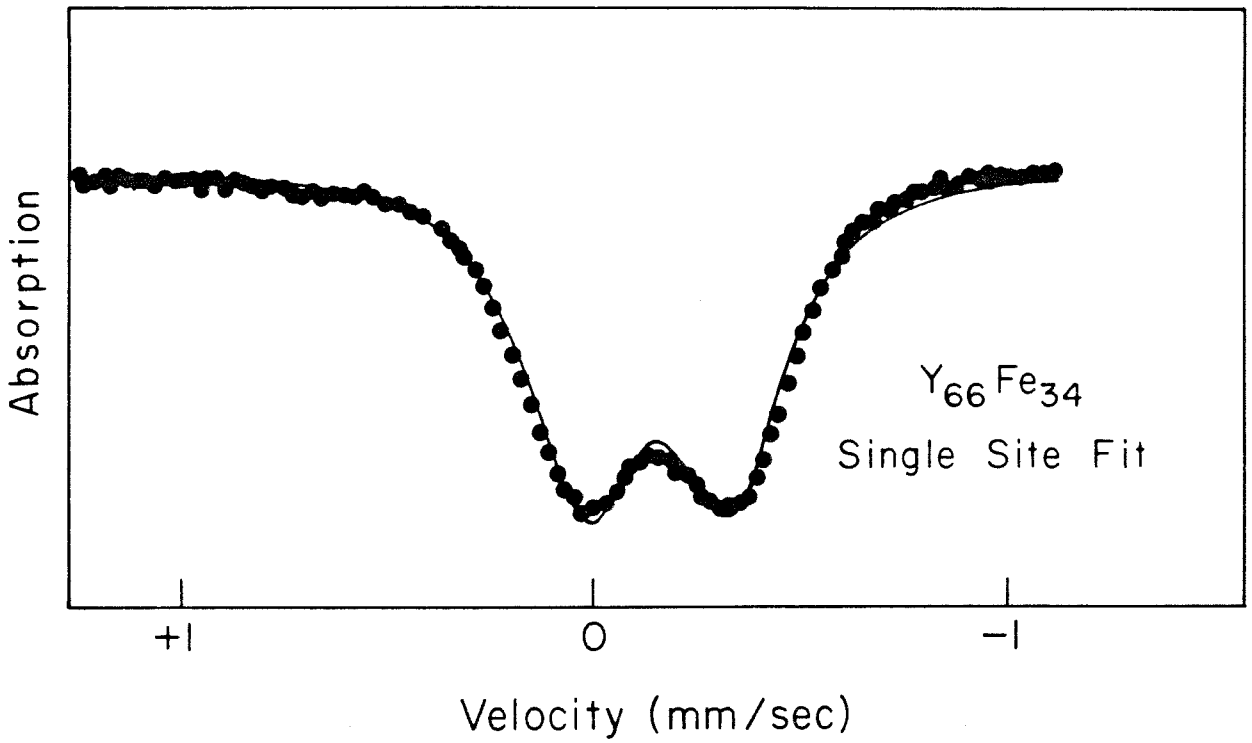

Fig. 15 The $Y_{66}Fe_{34}$ data from fig. 12 fit assuming one Fe site.

Table I ME parameters for $Y_{66}(Fe_{0.05}TM_{0.95})_{34}$ metallic glasses.

TM	QS-1 (mm/sec)	QS-2 (mm/sec)	IS-1* (mm/sec)	IS-2* (mm/sec)	Linewidth (mm/sec)	I_1/I_2
Mn	0.467(8)	0.174(8)	-0.153(8)	-0.094(8)	0.29(1)	0.89
Fe	0.472	0.226	-0.164	-0.165	0.28	1.07
Co	0.490	0.225	-0.162	-0.170	0.29	1.04
Ni	0.508	0.286	-0.158	-0.160	0.28	1.08
Cu	0.595	0.358	-0.174	-0.178	0.30	1.12
Zn	0.730	0.443	-0.152	-0.138	0.32	0.75

*IS values are with respect to α-Fe.

Table II ME parameters for $Y_{66}(Fe_yTM_{1-y})_{34}$ metallic glasses.

TM	y	QS-1 (mm/sec)	QS-2 (mm/sec)	IS-1 (mm/sec)	IS-2 (mm/sec)	Linewidth (mm/sec)	I_1/I_2
Mn	0.25	0.468(8)	0.180(8)	-0.155(8)	-0.113(8)	0.29(1)	0.88
Mn	0.50	0.466	0.192	-0.157	-0.130	0.29	0.96
Mn	0.75	0.467	0.212	-0.160	-0.147	0.28	0.95
Co	0.25	0.507	0.229	-0.158	-0.168	0.28	1.03
Co	0.50	0.513	0.238	-0.162	-0.160	0.28	0.95
Ni	0.25	0.504	0.253	-0.152	-0.158	0.28	1.08
Ni	0.50	0.494	0.242	-0.160	-0.160	0.28	1.08
Cu	0.30	0.595	0.284	-0.177	-0.177	0.31	0.91
Cu	0.50	0.582	0.272	-0.175	-0.175	0.30	0.89
Cu	0.70	0.536	0.266	-0.169	-0.174	0.29	1.13

characterized by its value of QS and IS. Site 1 is taken simply as the site having the larger value of QS. As an approximation we have assumed that the Γ values of the two sites are the same. The Γ values obtained as mentioned before are quite narrow and only slightly larger than what one expects to find in a single phase crystalline material of comparable Fe^{57} thickness. For TM = Mn, Fe, Co, and Ni we find that the various parameters (QS-1, QS-2, IS-1, IS-2) vary in a smooth monotonic fashion with composition. This coupled with the observation that the ratio of the intensities of the two sites is always about 1 shows that Fe randomly substitutes for the other TM's in the glassy structure. With this in mind we now focus our attention on the $Y_{66}(Fe_{0.05}TM_{0.95})_{34}$ data (Table I) with some confidence that our Fe probe occupies the sites normally occupied by the various TM's in the binary glasses $Y_{66}TM_{34}$. This appears to be true for the TM = Mn, Fe, Co, and Ni cases, we will comment on the TM = Cu and Zn cases later.

As fig. 16 shows, the behavior of the spectra is radically different depending on whether TM is to the right of left of Ni. We will concentrate on the systems TM = Mn, Fe, Co, and Ni first. Looking at fig. 16 and Table I we see that QS-1 and IS-1 are relatively weak functions of the identity of TM while QS-2 and IS-2 are somewhat more sensitive to TM. In fact, the visible changes we see in the spectra as TM goes from Mn to Ni are attributable primarily to the dependence of IS-2 on TM. For TM = Cu and Zn dramatic changes in the ME parameters of both site 1 and site 2 occur. QS-1 and QS-2 are much higher (see fig 16) than the values found for elements to the left of Cu. The fact that

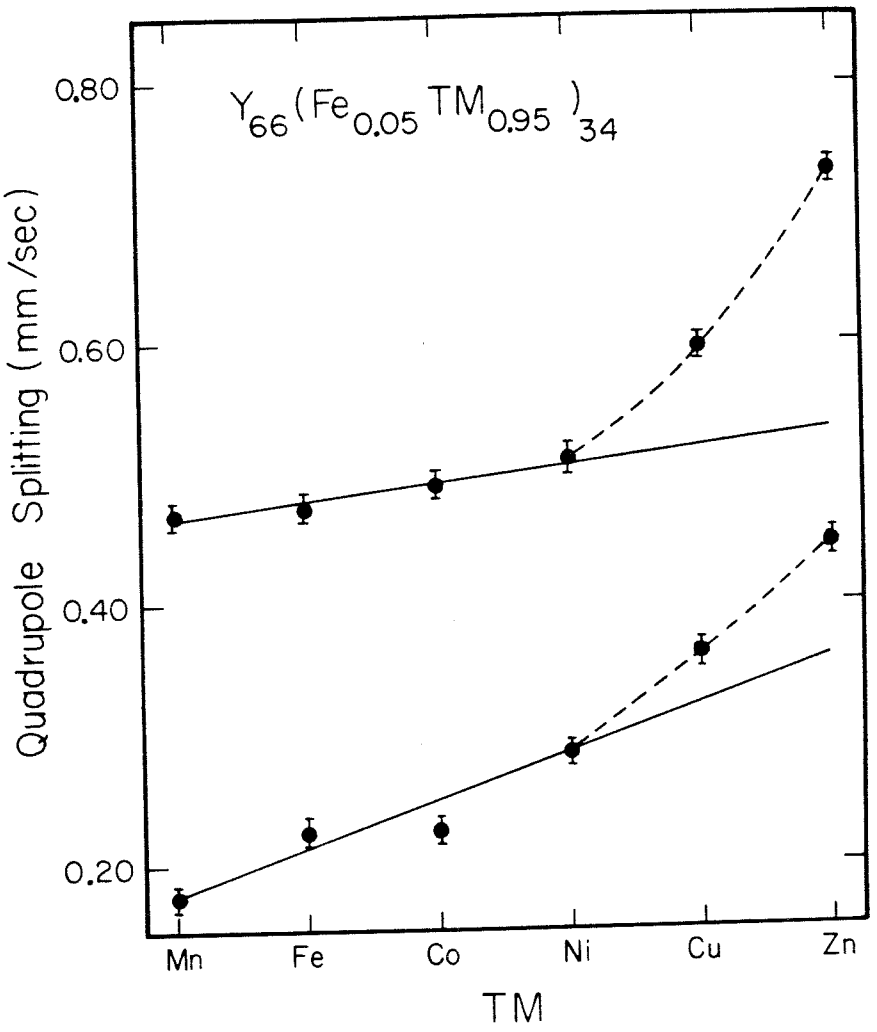

Fig. 16 The QS values for site 1 (top curve) and site 2 (lower curve) for $Y_{66}(Fe_{0.05}TM_{0.95})_{34}$ metallic glasses obtained by fitting the ME spectra to two Fe sites. The solid and dashed lines were put in as an aid in viewing the data.

we see changes in both the sites with y indicates that the nature of the two sites is changing as Cu and Zn are added.

ME spectra of the crystalline Laves (C-15) phase compounds $Y(Fe_{0.05}TM_{0.95})_2$ and $Y(Fe_xMn_{1-x})_2$ consisted of two distinct lines. The spectrum of TM = Co was shown in fig. 6. The ME parameters derived from fitting these crystalline alloys are listed in Table III. For TM = Ni, the linewidth is somewhat large. This may mean that the alloy was not homogeneous or that there are problems ordering this composition. Comparing Table I and Table III, we see an interesting correlation between the parameters of site 2 (for Mn, Fe, Co, and Ni) and the QS and IS of the corresponding C-15 compound. Note that the changes in QS and IS in going from Mn to Ni are in the same direction as in site 2, but that the changes are larger in magnitude for the crystalline samples.

Because of the success we had in fitting the $Y_{66}(Fe_yTM_{1-y})_{34}$ ME spectra to two Fe sites, we tried the same kind of analysis for the $Y_{1-x}Fe_x$ glasses. In fig. 17 we show the results of fitting the x=0.34 and x=0.40 spectra to two sites. The various parameters are listed in Table IV and the QS's and IS's are plotted in fig. 18. The compositional dependence of IS and QS for the two sites is noticeably different. For site 1 we see that QS is independent of x and that IS varies smoothly with x. Site 2, on the other hand, has sharp changes in QS and IS occuring at about x=0.36. Comparing fig. 18 with the results of the one site fits (fig. 11) we see that the changes in QS with x originate just from the changes in site 2 while the changes

Table III ME data on the C-15 compounds $Y(Fe_{0.05}TM_{0.95})_2$.

TM	IS (mm/sec)	QS (mm/sec)	Linewidth (mm/sec)
Mn	-0.020(7)	0.218(7)	0.24(1)
Fe	-0.122	0.480	0.28
Co	-0.135	0.466	0.26
Ni	-0.130	0.553	0.32

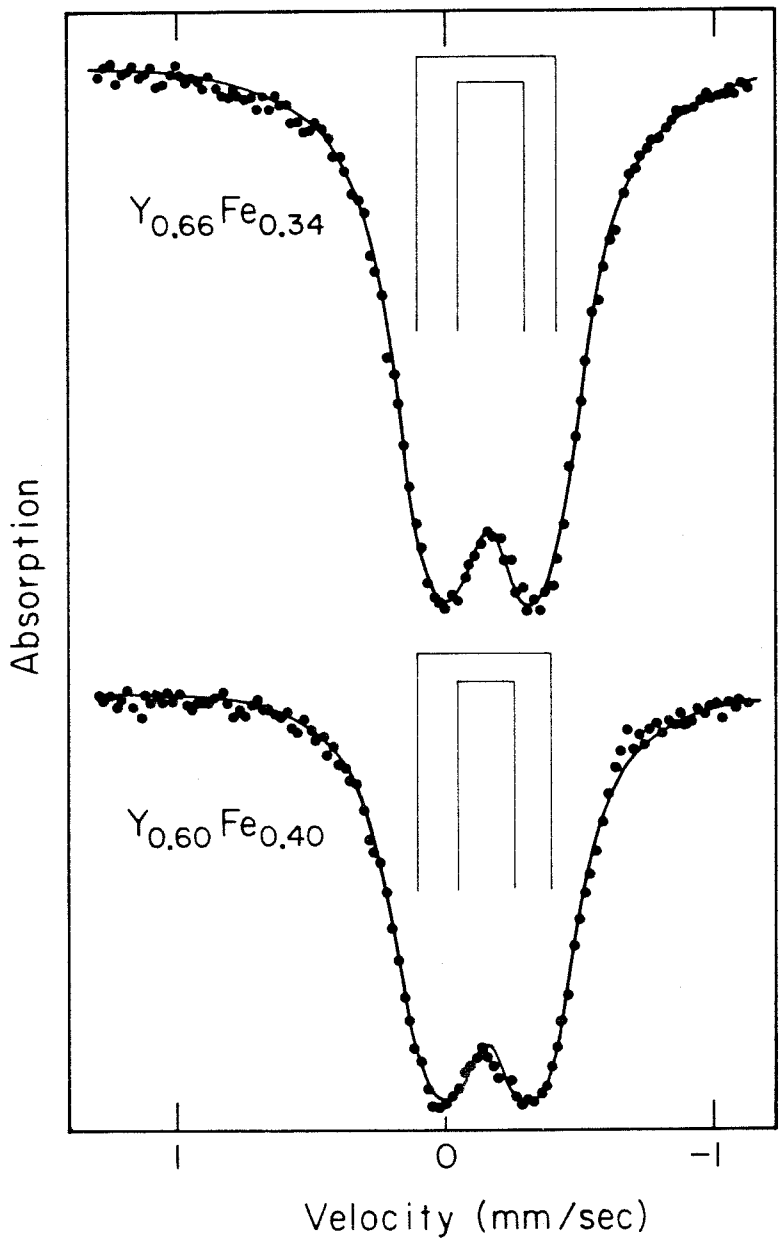

Fig. 17 The ME spectra of the glasses $Y_{0.66}Fe_{0.34}$ and $Y_{0.60}Fe_{0.40}$ fitted to two Fe sites.

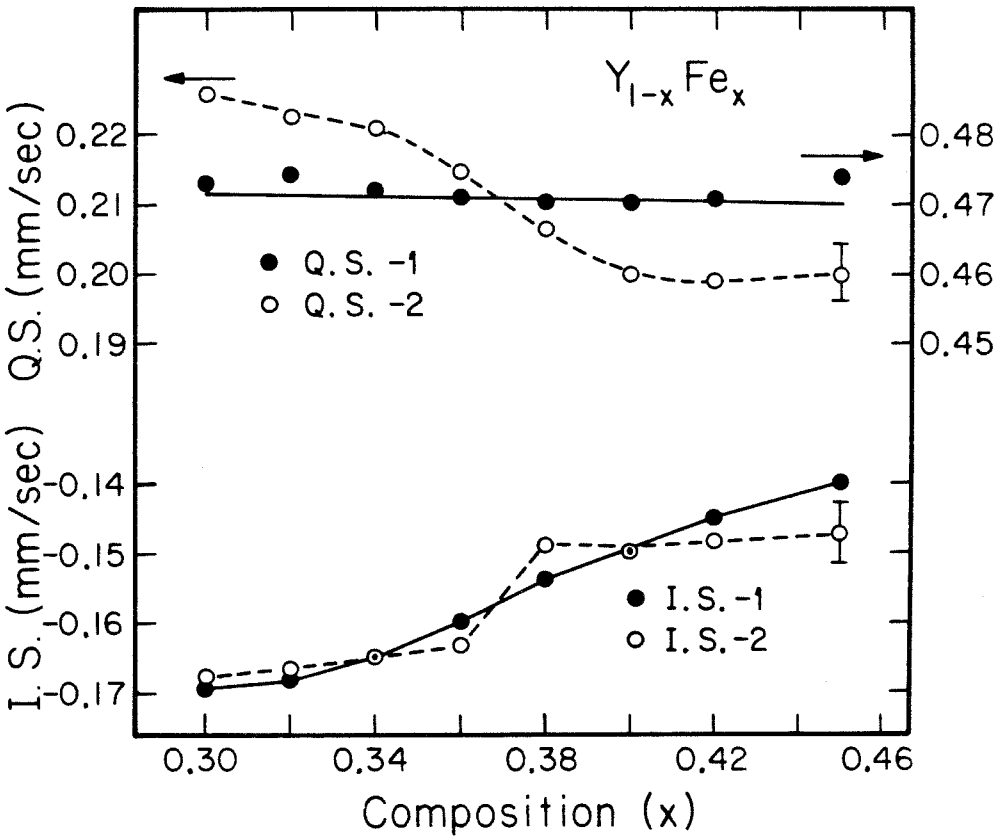

Fig. 18 The results of fitting the ME spectra of the $Y_{1-x}Fe_x$ glasses to two Fe sites.

Table IV Results of using the two site model on the ME spectra of $Y_{1-x}Fe_x$ glasses.

x	QS-1 (mm/sec)	QS-2 (mm/sec)	IS-1 (mm/sec)	IS-2 (mm/sec)	Linewidth (mm/sec)	I_1/I_2
0.30	0.473(5)	0.226(5)	-0.169(5)	-0.168(5)	0.29	0.94
0.32	0.474	0.223	-0.168	-0.167	0.28	1.05
0.34	0.472	0.221	-0.165	-0.165	0.27	1.04
0.36	0.471	0.215	-0.160	-0.163	0.29	1.01
0.38	0.470	0.207	-0.154	-0.149	0.26	1.04
0.40	0.470	0.200	-0.150	-0.150	0.26	1.04
0.42	0.471	0.199	-0.145	-0.148	0.27	1.17
0.45	0.474	0.200	-0.140	-0.147	0.29	1.23

in IS with x has contributions from both sites.

Combining the results for the metallic glasses $Y_{66}(Fe_yTM_{1-y})_{34}$ (TM = Mn, Fe, Co, and Ni) and $Y_{1-x}Fe_x$, we have found that the ME spectra can best be understood in terms of a model which assumes two Fe sites. The Fe site designated site 2 was found to be sensitive to the identity of TM and to the composition x. In contrast, site 1 was less sensitive to the identity of TM. The QS of site 1 was found to be independent of x while its IS smoothly varied with x.

C. Crystallization of Y-Fe Glasses

In fig. 19 we show the results of a typical DSC and high temperature resistivity measurement on a $Y_{0.66}Fe_{0.34}$ metallic glass. In both these measurements we see evidence of two irreversible transformations occurring at approximately 580 K and 700 K. From X-ray diffraction measurements on heat treated foils we find that the transformation occurring at about 580 K is the formation of hcp Y and the transformation occurring at about 700 K is the formation of the C-15 compound YFe_2. These are the two equilibrium phases for this composition. The Bragg reflections of the hcp Y phase formed by the low temperature annealing (less than 680 K) are very broad which indicates that the crystals which have formed are small in size. The effective microcrystal size estimated from the widths of the Bragg peaks is 20 nm. The hcp Y peaks do not begin to sharpen up until the final step in the crystallization occurs (the formation of YFe_2). We found that all the $Y_{1-x}Fe_x$ glasses behaved the same upon annealing and we will concentrate on the value x=0.34. See fig. 20 for the X-ray patterns of two heat treated

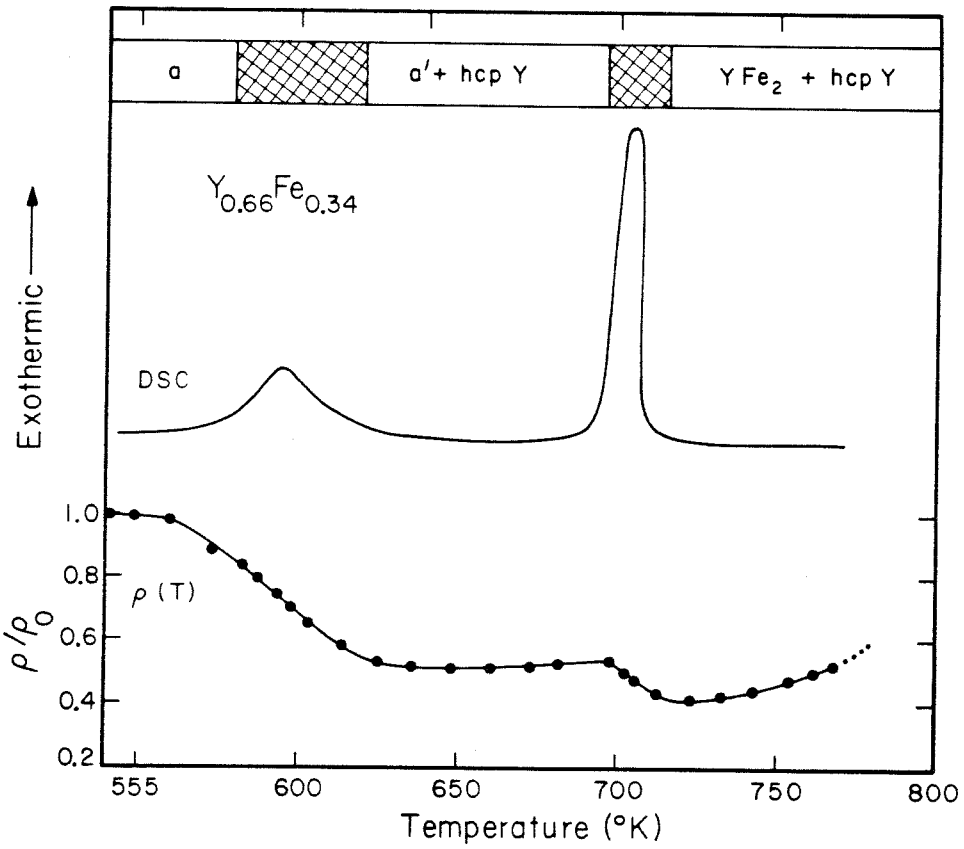

Fig. 19 DSC and high temperature resistivity ($\rho(T)$) measurements on the metallic glass $Y_{0.66}Fe_{0.34}$. The values of $\rho(T)$ have been normalized by the value of ρ at room temperature (ρ_0 = 270 $\mu\Omega$-cm). The designations a and a' refer to completely amorphous (a) and to the Fe enriched amorphous phase (a') which remains as hcp Y is formed.

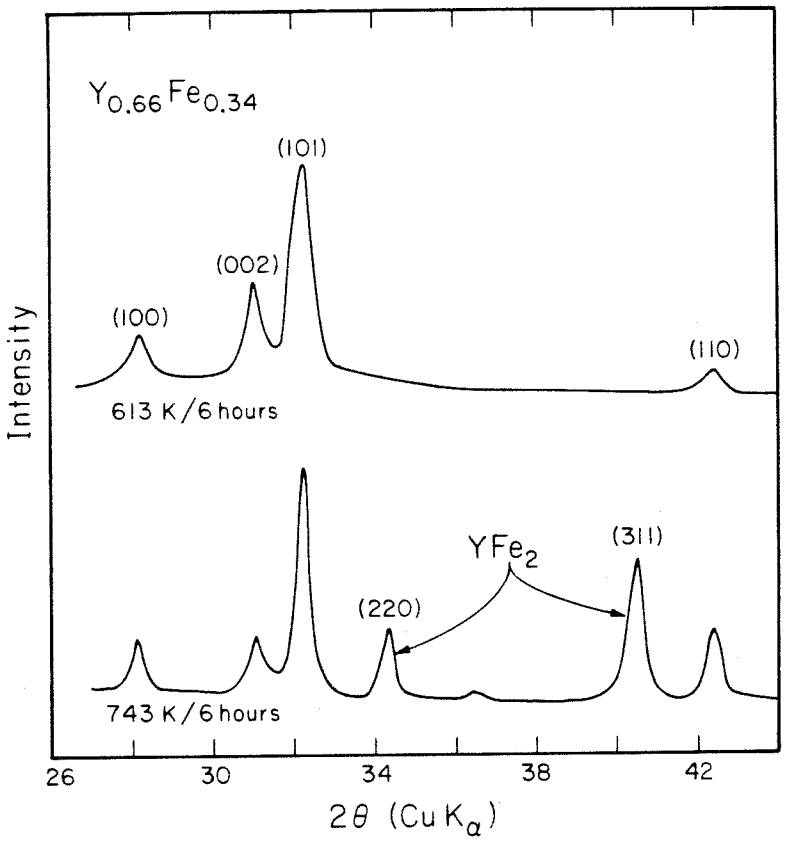

Fig. 20 X-ray diffraction patterns of two heat treated $Y_{0.66}Fe_{0.34}$ foils. The top pattern identifies the Bragg reflections of hcp Y and the bottom pattern shows the additional reflections of C-15 YFe_2.

$Y_{0.66}Fe_{0.34}$ foils.

In fig. 21 we show the results of the ME experiments on a $Y_{0.66}Fe_{0.34}$ foil which has been heat treated at various temperatures (T_A) for 6 hours. In this particular set of experiments the same foil was used for all the measurements so that the heat treatments are additive. For $T_A < 650$ K, the ME spectra consist of two well defined lines. These spectra were least squares fitted to two Lorentzian lines having the same linewidth. We see in fig. 21 that this approach provides a good fit of the experimental data. Earlier we found that the spectra of the as-quenched glasses was actually composed of two contributions. The heat treated foils seem to be more complicated than the as-quenched glasses and the two site approach does not seem applicable. We will discuss this point later. For the purposes of this study, the two Lorentzian approach used for the first two spectra of fig. 21 is adequate if we keep in mind that the values of QS and IS we obtain represent average values.

For $T_A > 650$ K the character of the spectra changes as additional lines begin to appear. These lines come from Fe atoms in a crystalline YFe_2 phase. This compound, unlike the amorphous phase, is ferromagnetic at room temperature and most of its contribution to the ME spectrum is beyond the velocity range scanned by the experiments of fig. 21. The $T_A = 743$ K spectrum is a fully crystallized sample in which all the Fe atoms are in the YFe_2 phase. In this compound, all the Fe sites are crystallographically equivalent and thus have the same IS and QS. The Fe sites however, are not magnetically equivalent and the ME spectrum

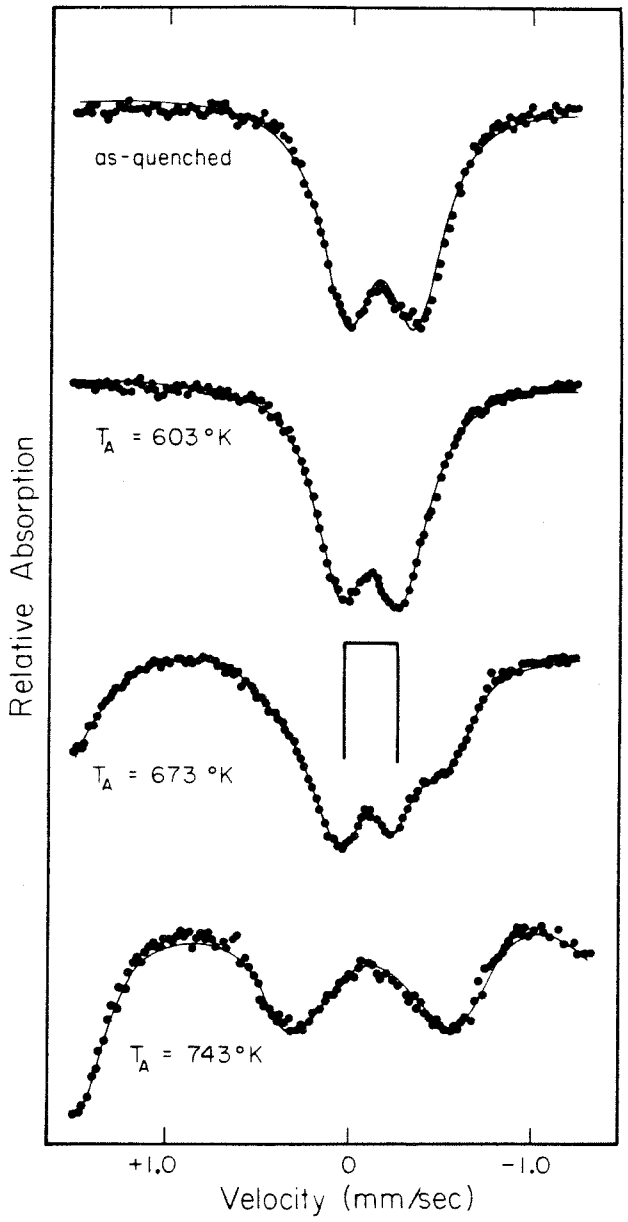

Fig. 21 ME spectra for a heat treated $Y_{0.66}Fe_{0.34}$ foil. The foil was treated at $T = T_A$ for 6 hours and the heat treatments are additive. The solid lines through the data points are the results of the least squares analysis. The results of these fits are listed in Table V as foil III.

of YFe_2 consists of two sets of six lines representing the two values of the internal magnetic hyperfine field (H_{int}). In YFe_2 the electric field gradient is axially symmetric (along the (111) direction) and the formula we mentioned earlier in discussing combined electric quadrupole-magnetic dipole interactions is appropriate. The parameters for the two Fe sites are H_{int} = 205 kOe , θ =70 and H_{int} = 180 kOe , θ = 0. The site having H_{int} = 205 kOe has three times the intensity of the other site. Because of the limited velocity range investigated and the small amount of YFe_2 in most of the samples, we were not able to completely characterize this compound for many of the annealed samples. We chose instead to fit the YFe_2 contribution to the spectra by the following procedure. In the velocity range investigated in fig 21, the two magnetic sub-spectra are each composed of three Lorentzian lines in which the two lines centered about zero velocity are constrained to have equal intensities. We also fix the ratio of the intensities of the two sub-spectra at 3/1 and the ratio of the values of H_{int} at 1.14/1. The result of this procedure is to determine the IS, average magnetic hyperfine field (H_{av}), and the total intensity of the YFe_2 contribution to the spectrum. We should note that the spacing between the inner two lines of each sub-spectra is independent of QS , so that the values of IS and H_{av} should be quite reliable. This procedure does not enable us to determine QS for the partially crystalline samples.

In fig. 21 we see that this method provides a reasonable fit of the experimental data for the completely crystallized (T_A = 743 K) sample. The T_A = 673 K spectrum is an example of a spectrum in which some of the

Fe atoms are in an amorphous phase and some are in the YFe_2 compound. In fig. 21 we show the results of least squares fitting the spectrum to a superposition of Fe in an amorphous phase (2 lines) and Fe in YFe_2 (6 lines). From this fit we determine the IS and QS of the amorphous phase (referred to as IS-a and QS-a), H_{av} and IS (referred to as IS-c) of the YFe_2 phase, and the relative intensities of the two phases. All spectra of this study could be understood in terms of the amorphous phase and the C-15 compound. The results of the fitting procedures are listed in Table V and are shown in fig. 21. Like the DSC and high temperature resistivity measurements we see changes in the ME parameters occurring at about 580 K and 700 K. For 580 K < T_A < 680 K no YFe_2 is formed and the changes we see in the ME parameters must be connected with the crystallization of hcp Y. The equilibrium solubility of Fe in hcp Y is less that 0.1at%. As we will describe later, we found that rapidly quenched Y-rich alloys (like $Y_{0.90}Fe_{0.10}$) could contain as much as 3 at% Fe dissolved interstitially in hcp Y. This interstitial solid solution could not be formed by the crystallization of a $Y_{0.75}Fe_{0.25}$ amorphous sample. From this we conclude that the hcp Y which is formed by the low temperature crystallization of our $Y_{0.66}Fe_{0.34}$ glass contains very little Fe. The recoil free fraction of the samples stays constant during the entire crystallization process. Careful ME and X-ray studies of heat treated samples show that there is a one to one correspondence between changes in the ME spectra and the appearance of hcp Y in the X-ray patterns. This correspondence demonstrates that the formation of hcp Y crystals in the glass requires the correlated moment of Y and Fe

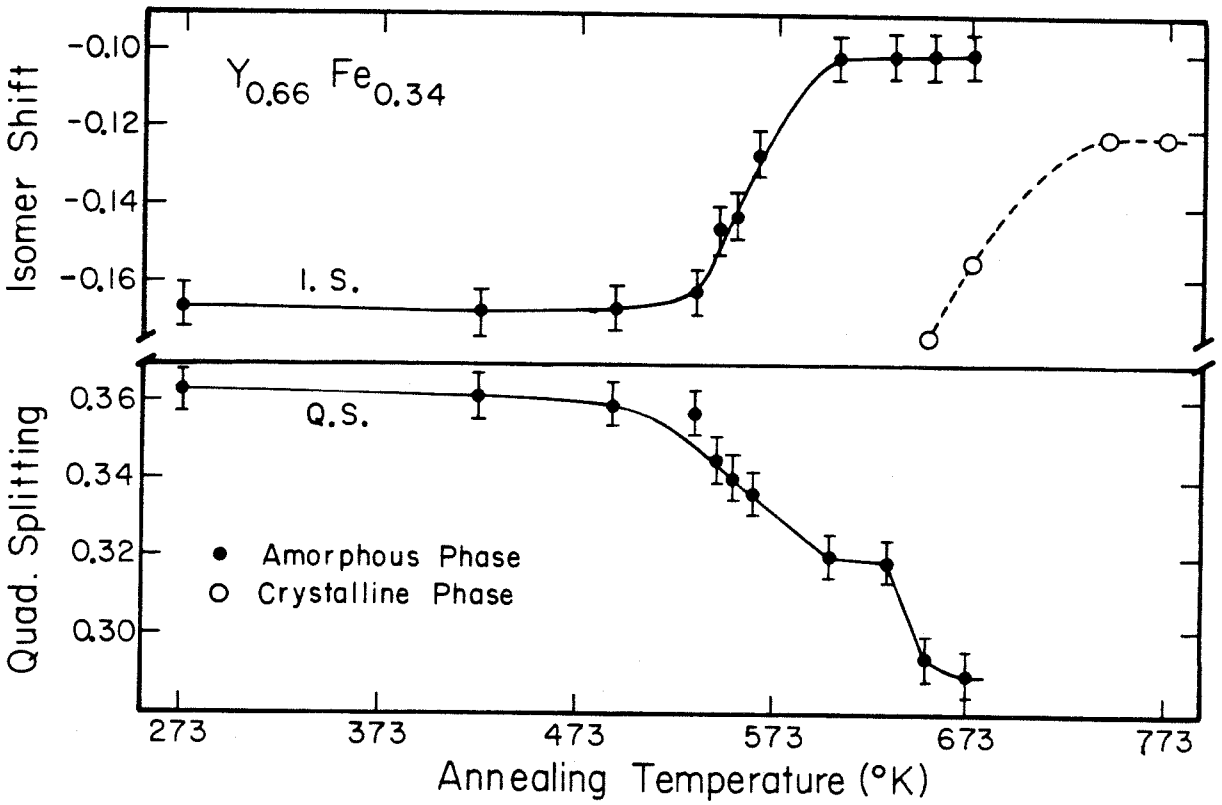

Fig. 22 The dependence of QS and IS in $Y_{0.66}Fe_{0.34}$ glasses on T_A for 6 hour heat treatments. The filled circles correspond to Fe atoms in an amorphous phase and the open circles refer to Fe atoms in the C-15 compound. The lines drawn through the data points were added as a guide in viewing the data.

Table V Results of ME experiments on $Y_{0.66}Fe_{0.34}$ foils annealed at $T=T_A$ for 6 hours. F_{YFe_2} is the fraction of Fe atoms in the C-15 phase.

Sample	T_A	QS-a (mm/sec)	IS-a (mm/sec)	IS-c (mm/sec)	H_{av} (kOe)	Linewidth (mm/sec)	F_{YFe_2}
Foil-I	as-quenched	0.362(6)	-0.166(6)	-	-	0.34(1)	-
"	423	0.361	-0.167	-	-	0.34	-
"	492	0.359	-0.166	-	-	0.36	-
"	533	0.357	-0.162	-	-	0.35	-
"	548	0.345	-0.145	-	-	0.34	-
Foil-II	as-quenched	0.359	-0.166	-	-	0.34	-
"	563	0.336	-0.128	-	-	0.35	-
"	652	0.295	-0.102	-0.173	144	0.36	0.55
Foil-III	as-quenched	0.364	-0.168	-	-	0.35	-
"	553	0.340	-0.143	-	-	0.36	-
"	603	0.315	-0.102	-	-	0.34	-
"	673	0.290	-0.101	-0.154	180	0.36	0.77
"	743	-	-	-0.122	205	0.36	1.00

atoms. As hcp Y is formed we expect the remaining amorphous phase to become richer in Fe. We illustrate this schematically in fig. 23 where we have reproduced our results on the compositional dependence of QS and IS for the $Y_{1-x}Fe_x$ glasses. We see that the behavior of IS-a and QS-a as a function of T_A is consistent with the idea that the amorphous phase is becoming richer in Fe as T_A increases. The IS scale is such that Fe metal corresponds to an IS of 0.00. The increase in IS-a with T_A is a consequence of the Fe atoms having progressively more Fe neighbors. This changing composition is the factor which makes the spectra of the annealed samples more complicated than the as-quenched glass spectra. As fig. 22 shows, the value of IS-a and QS-a saturate for T_A greater than 600 K. Continued annealing (up to 14 days) at T_A = 600 K does not result in further changes in IS-a or QS-a. It seems that the remaining amorphous phase (RAP) has reached its maximum Fe content at this point. Note that the total change in IS and QS with annealing is about a factor of two larger tha we observed in the compositional studies in $Y_{1-x}Fe_x$. From this we conclude that the final composition of the RAP is richer in Fe than the Fe richest glass of that study ($Y_{0.55}Fe_{0.45}$). The annealing process has thus produced a non-crystalline phase which is not accessible by standard liquid quenching techniques. The Fe content of the RAP may be as high as 66 at%.

For values of T_A greater that 680 K we begin to see contributions from Fe atoms in the YFe_2 phase in the spectra. In Table V we listed the results of the fitting procedure for some of these samples. Of special interest is the behavior of IS-c and H_{av} with T_A. We see that

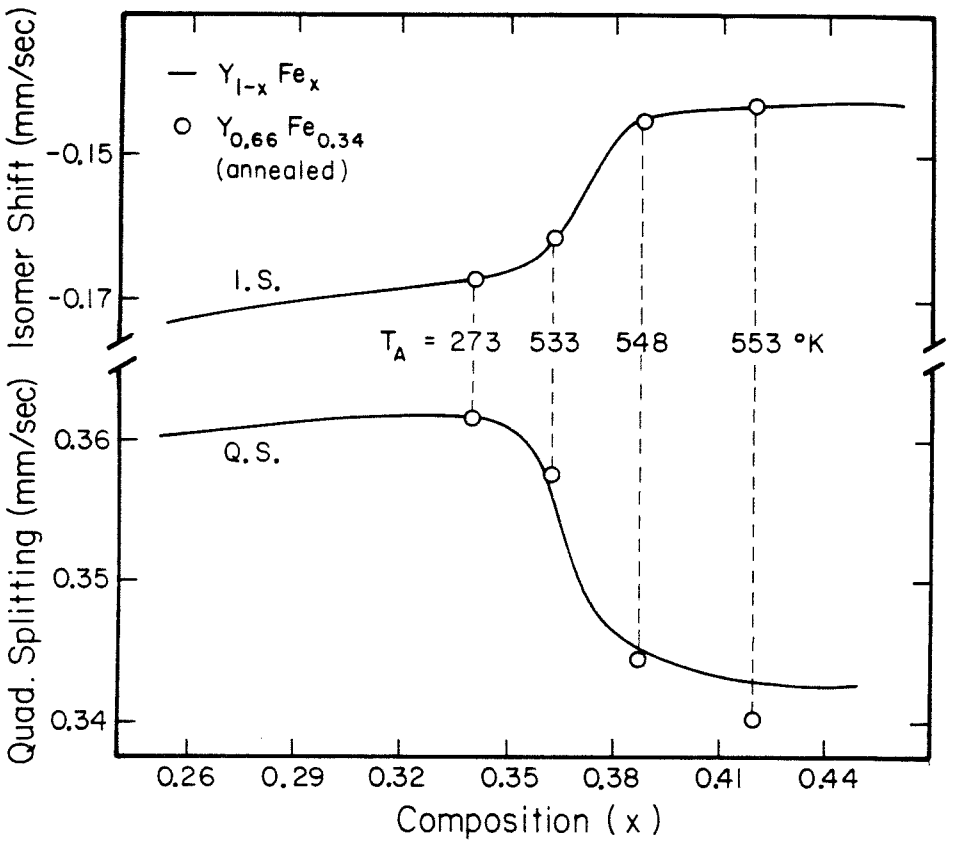

Fig. 23 A schematic illustration of the changing composition of the amorphous phase with T_A. All heat treatments are for 6 hours. The solid lines reproduce the values of QS and IS for the glasses $Y_{1-x}Fe_x$ from fig. 11. We estimate the value of x of the annealed sample by comparing its IS to the IS's of the $Y_{1-x}Fe_x$ system. Using this estimate of x we then plot its QS and compare it with the QS values from the $Y_{1-x}Fe_x$ system.

the YFe_2 which is formed initially (T_A = 652 K) has a significantly smaller IS and H_{av} than the fully crystallized sample (T_A = 743 K). The increase in IS-c and H_{av} with T_A leads us to conclude that the YFe_2 formed at lower values of T_A has some Fe vacancies. It has been found that the substitution of nonmagnetic elements like Al for Fe in YFe_2 reduces H_{av} [21]. This reduction is approximately 14% for each nonmagnetic near neighbor about an Fe site. It is reasonable to expect that the effect of an Fe vacancy will be similar to that of having a nonmagnetic near neighbor. From this we estimate that the YFe_2 forms initially with two Fe vacancies. With higher values of T_A these vacancies disappear and IS-c and H_{av} reach their proper values. The IS difference between the RAP and the YFe_2 compound is readily apparent from the asymmetric nature of the T_A = 673 K spectrum in the region near zero velocity in fig. 21. In fig. 22 we see that the final value of IS-c is lower than the value at which the RAP saturates. This is a very important observation as it provides some estimate of the amount of chemical short range order in the RAP. In crystalline YFe_2, Fe has 6 Fe and 6 Y near neighbors which is about two more Y near neighbors than is expected from a random arrangement of Y and Fe atoms. The higher IS of the amorphous phase compared to YFe_2 suggest that the chemical ordering in the C-15 compound is relaxed to some extent in the amorphous phase. IS-a is higher that IS-c because of the larger number of Fe near neighbors in the RAP compared to the crystalline phase. We estimate that Fe has something like 8 Fe near neighbors in the RAP. We also note that the QS of the YFe_2 compound (0.480 mm/sec) is very different

from the final value of QS-a. With these observations in mind, we conclude that the chemical and topological short range order in the RAP is different from that which exist in YFe_2 . In particular, the RAP appears to lack chemical order and the topological environment seems to be less distorted than in the crystal. Referring back to fig. 18 we saw a change in IS-2 of the $Y_{1-x}Fe_x$ glasses as a function of x which we identified as resulting from the substitution of one Y near neighbor by an Fe atom. If we assume that the RAP has 8 Fe near neighbors and that a change of IS-2 by 0.016 mm/sec corresponds to the replacement of a Y near neighbor by an Fe atom (from fig. 18), then we find that the number of Fe-Fe neighbors in the as-quenched $Y_{0.66}Fe_{0.34}$ glass is 4. This is the number of Fe-Fe near neighbors we would expect from a random arrangement of Y and Fe atoms.

In our analysis of the $T_A < 680$ K spectra we avoided the use of the two site fits we found so successful for the as-quenched samples. We did this because we believed that this would not be a reliable way of understanding the data due to the complex nature of the partially crystalline samples. Crystallization is an inhomogeneous process and leads to compositional gradients in the samples. The increase in line-width upon heat treatment we see for the $Y_{0.66}Fe_{0.34}$ samples illustrates this point (Table V). For $T_A > 600$ K (but no formation of YFe_2) we saw that the IS and QS curves saturated indicating that this represents the final condition of the RAP. In Table VI we list the results of fitting the spectra of an as-quenched and a heat treated sample in the saturated region to two sites. The interesting feature of this analysis is that

Table VI Results of ME experiments on heat treated $Y_{66}(Fe_yMn_{1-y})_{34}$ glasses.

y	Condition	QS-1 (mm/sec)	QS-2* (mm/sec)	IS-1 (mm/sec)	IS-2* (mm/sec)	Linewidth (mm/sec)	I_1/I_2
0.05	as-quenched	0.468(8)	0.174(8)	-0.153(8)	-0.094(8)	0.29(1)	0.89
0.05	RAP + hcp Y	0.470	0.154	-0.116	-0.122	0.27	0.55
0.05	C-15 + hcp Y	-	0.218	-	-0.020	0.24	-
0.50	as-quenched	0.465	0.189	-0.157	-0.131	0.26	0.97
0.50	RAP + hcp Y	0.455	0.170	-0.120	-0.126	0.25	0.50
0.50	C-15 + hcp Y	-	0.250	-	-0.069	0.24	-
1.00	as-quenched	0.472	0.226	-0.165	-0.164	0.28	1.07
1.00	RAP + hcp Y	0.468	0.199	-0.102	-0.104	0.28	0.58
1.00	C-15 + hcp Y	-	0.480	-	-0.122	0.30	-

*IS-2 = IS and QS-2 = QS for C-15 compounds.

the intensity ratio decreased to about 0.50 in the RAP sample. We have also studied the crystallization of $Y_{66}(Fe_yMn_{1-y})_{34}$ (y=0.05 and 0.50) glasses. The equilibrium phases for the Mn containing samples are the same as the Y-Fe samples (hcp Y and a C-15 compound). The X-ray diffraction results indicate that the crystallization of the Mn containing glasses is identical to that of the Y-Fe glasses. After a 600 K/ 6 hours anneal the IS and QS values of these samples saturate until the final step in the crystallization process occurs. In Table VI we list the results of the two site fits for these samples. Again, we see that the intensity ratio has decreased to about 0.50. Note the different behavior of IS-2 for the three alloys and the difference between the final values of IS-2 and the corresponding C-15 compound. This apparent discrepancy will be addressed later in the discussion section. For the moment let us ignore the behavior of IS-2 of the Mn containing samples. We see that QS-1 is essentially the same between as-quenched and annealed samples while QS-2 is noticeably smaller after annealing for all three compositions.

In an attempt to estimate the effective activation energies of the two crystallization processes we performed several series of isothermal annealing experiments. Foils of $Y_{0.66}Fe_{0.34}$ were mounted in the high temperature ME furnace and spectra were recorded as a function of time for various values of T_A. For the formation of hcp Y we use IS-a as a measure of the extent of crystallization and for the formation of YFe_2 we use the measured fraction of amorphous and crystalline material. In these experiments we determine the time required for half the material

to transform ($\tau_{\frac{1}{2}}$). If we assume that we can describe these processes by a simple Arrhenius behavior then we can write

$$\tau_{\frac{1}{2}} = \tau_o \exp(\Delta/k_B T)$$

We show the results of this procedure in fig. 24 where we find that the activation energy (Δ) associated with the process of the formation of hcp Y and YFe_2 are 2.2 ev and 3.6 ev respectively.

D. Rapidly Quenched $Y_{1-x}Fe_x$ Solid Solutions

In our discussion of the $Y_{1-x}Fe_x$ system we mentioned that for x less than 0.25 the as-quenched foils were partially crystalline. Giessen et al[22] reported that rapidly quenched Y-Cu and Y-Fe alloys formed novel metallic solid solutions. These solid solutions were of a kind not previously reported for metallic alloys. Cu and Fe were claimed to form interstitial solid solutions with Y. These solid solutions were remarkable in that they contained up to 15 at% of the small atom with neglible changes in the lattice parameters.

The X-ray diffraction patterns of the majority of our $x < 0.25$ rapidly quenched samples consisted of an amorphous band and a hcp phase. The X-ray diffraction patterns of a x=0.25 and x=0.10 sample were shown in fig. 7. Some of the as-quenched foils had X-ray patterns which consisted of only the Bragg peaks of hcp Y. We will refer to these samples as quenched-hcp (q-hcp) samples. The hcp peaks we find for the q-hcp samples are very broad indicating small crystal size and/or internal stress in the samples. Because of this fact, accurate lattice

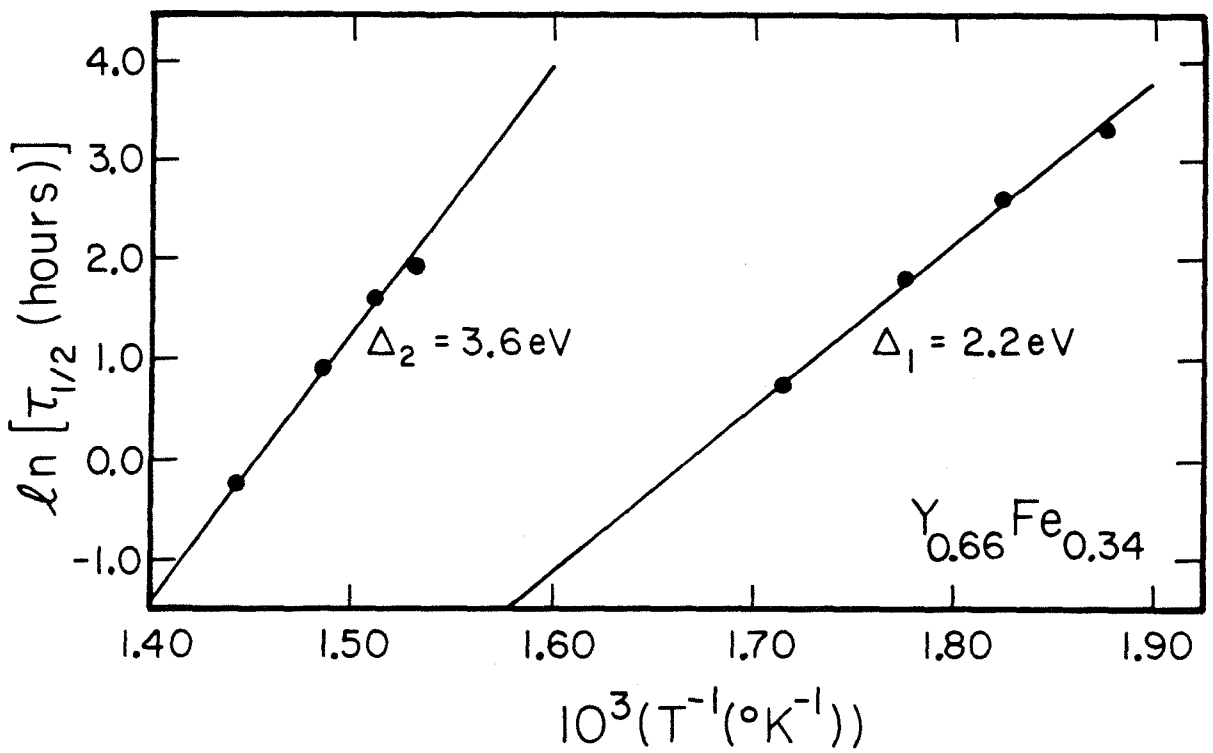

Fig. 24 Arrhenius plots to determine the effective activation energies for the formation of hcp Y (Δ_1) and YFe_2 (Δ_2). The straight lines are least squares fits of the points from which we extract the activation energies.

parameter measurements are difficult. The lattice parameters of the q-hcp samples seem to be independent of x (c = 0.574 nm and a = 0.365 nm) and are slightly larger than those of pure hcp Y metal (c = 0.5731 nm and a = 0.3647 nm).

In fig. 25 we show the results of our density measurements on these samples. We see that the q-hcp samples have atomic densities which are in good agreement with the calculated values for Fe dissolved interstitially in hcp Y (dotted line). Similar results by Giessen et al[22] for density and X-ray measurements led them to conclude that Fe and Cu form interstitial solid solutions with Y. We also see in fig. 25 that the density of completely amorphous samples and even as-cast alloys are the same as the q-hcp samples. From these observations we see that density measurements in this system cannot distinguish between the various states of the samples. Giessen et al[22] only measured the rapidly quenched foils and therefore did not compare them with the as-cast alloys.

In Table VII we show the results of ME experiments on these samples. Here, we see some clear differences between the q-hcp and amorphous samples. All as-cast samples had ME spectra which consisted of the 12 line magnetic hyperfine structure of the C-15 compound YFe_2. The samples listed in Table VII all had ME spectra which were composed of two equally intense lines (see fig. 27). These spectra were least squares fitted to two Lorentzians which were constrained to have the same line-width. From Table VII we see that the QS and IS of all the quenched foils are similar. The most striking difference between the various

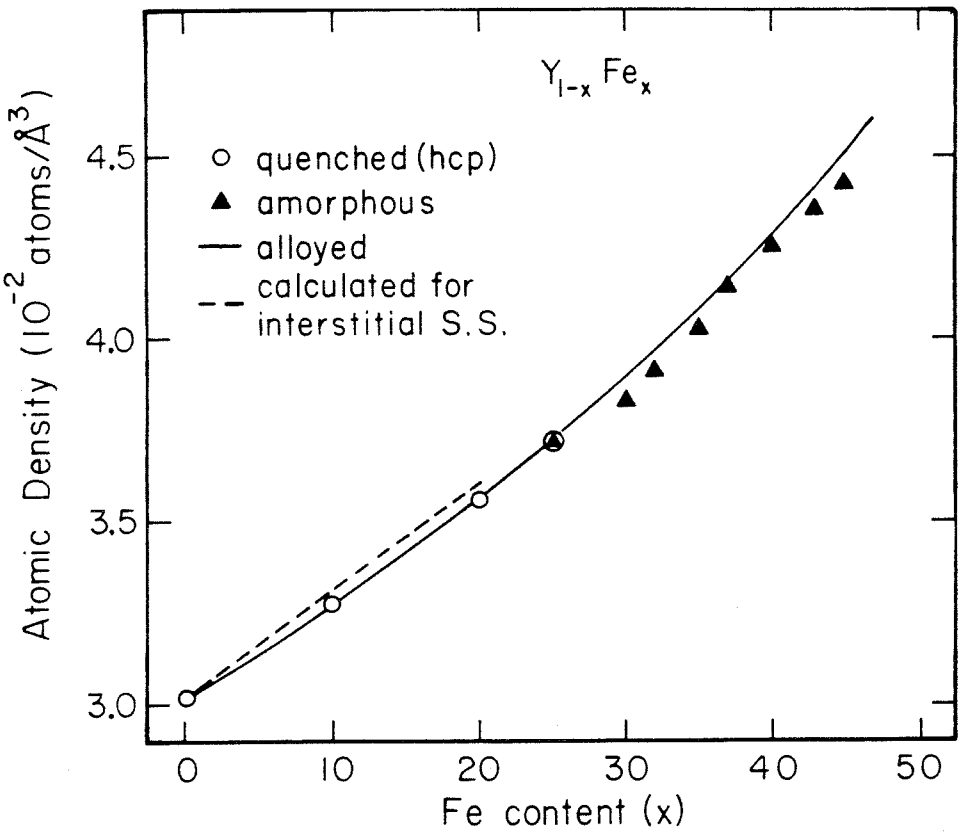

Fig. 25 Atomic Density of rapidly quenched and crystalline $Y_{1-x}Fe_x$ samples. The solid line represents the measurements on as-cast ingots measured at intervals of 5 at%.

Table VII Summary of ME data on rapidly quenched $Y_{1-x}Fe_x$ and $Y_{0.90}Cu_{0.10-z}Fe_z$.

Sample	Condition	Area*	QS (mm/sec)	IS (mm/sec)	Linewidth (mm/sec)	f/f_{Fe}
x=0.30	amorphous	1.01(2)	0.366(3)	-0.169(3)	0.36(1)	0.65
x=0.30	a + q-hcp	1.18	0.343	-0.149	0.37	0.76
x=0.25	amorphous	1.00	0.379	-0.173	0.36	0.66
x=0.25	q-hcp	1.31	0.321	-0.149	0.37	0.83
x=0.10	q-hcp	1.70	0.323	-0.134	0.36	1.13
z=0.05	q-hcp	1.51	0.348	-0.160	0.36	1.00
z=0.02	q-hcp	1.60	0.365	-0.156	0.35	1.06

*normalized to be 1.00 for the amorphous $Y_{0.75}Fe_{0.25}$ sample.

samples is in the area under resonance. Those samples containing some of the q-hcp phase have larger areas than the amorphous or as-cast samples. As we mentioned previously, the area under resonance of a ME spectrum in the thin absorber limit is proportional to the recoil free fraction (f). In a harmonic solid we can write for the recoil free fraction $f = \exp(-E_\gamma^2 \langle x^2 \rangle / (\hbar c)^2)$, where $\langle x^2 \rangle$ is the mean square displacement of the resonant atom. In Table VII we have normalized the f values of our samples to that of pure Fe metal. We find that f/f_{Fe} for samples containing the q-hcp phase is significantly higher than that of the amorphous or as-cast alloys. Similar anomalously high values of f were found by Flinn et al[23] for very dilute Co^{57} impurities diffused into In. We suggest that the high values of f (and therefore small values of $\langle x^2 \rangle$) of our samples are a consequence of having some of the Fe atoms in interstitial sites.

The experiments on heat treated samples are the key to understanding these materials. DSC scans of amorphous and q-hcp samples consisted of two exothermic peaks at about 580 K and 700 K. This similarity suggests that the q-hcp samples contain some amorphous material. From sub-section C we know (from our work on amorphous $Y_{0.66}Fe_{0.34}$) that the first peak in the DSC is associated with the primary crystallization of hcp Y and the second peak is related to the formation of the compound YFe_2. In Table VIII we display the ME parameters of heat treated samples of amorphous $Y_{0.75}Fe_{0.25}$, q-hcp $Y_{0.75}Fe_{0.25}$, and q-hcp $Y_{0.90}Fe_{0.10}$. From the results of our work on the crystallization of $Y_{0.66}Fe_{0.34}$ the behavior of the ME spectra of the amorphous sample with annealing

temperature (T_A) is clear. For $T_A > 600$ K we begin to see the formation of hcp Y leaving behind an Fe rich amorphous phase. As the amorphous phase becomes richer in Fe the IS steadily moves to the value -0.10 mm/sec and the QS decreases. After the T_A = 633 K treatment the X-ray diffraction pattern contains only the reflections of hcp Y. It is interesting to note that the density and X-ray diffraction patterns of a virgin q-hcp sample and 633 K/6 hours amorphous $Y_{0.75}Fe_{0.25}$ sample are identical.

We see that the behavior of QS and IS with T_A is the same for all three samples, the only difference being in the initial values. An important difference is found in the area under resonance of the ME spectra of the three samples. We illustrate the dependence of the area on T_A for the samples in fig. 26. The area of the amorphous sample stays approximately constant through complete crystallization while the q-hcp samples suffer a drastic decrease in area. The area under resonance decreases to the same value as the amorphous samples. This demonstrates that the high f site in the virgin samples decomposes at about 633 K (360°C) and that the interstitial site is not formed by the low temperature crystallization of the amorphous phase. We show the ME spectra of the q-hcp $Y_{0.90}Fe_{0.10}$ for several values of T_A in fig. 27. The drop in area we mentioned above can clearly be seen in the spectra. Examining the high velocity features of the spectra (where the YFe_2 compound makes its largest contribution to the spectrum) we find that less Fe is in the YFe_2 compound than was originally in the high f site. This leads to the interesting conclusion that some of the Fe atoms must have gone from the interstitial site to the amorphous phase. The fact

Table VIII Results of ME experiments on heat treated $Y_{1-x}Fe_x$ foils.

Sample	Condition*	T_A^+(K)	Area++	QS (mm/sec)	IS (mm/sec)
a-0.25	amorphous	273	1.00(2)	0.379(6)	-0.173(6)
a-0.25	a + hcp Y	573	0.99	0.352	-0.152
a-0.25	hcp Y	633	0.99	0.306	-0.110
q-0.25	hcp Y	273	1.31	0.321	-0.149
q-0.25	hcp Y	573	1.29	0.322	-0.139
q-0.25	hcp Y	633	1.03	0.310	-0.102
q-0.10	hcp Y	273	1.70	0.323	-0.134
q-0.10	hcp Y	573	1.69	0.312	-0.133
q-0.10	hcp Y	633	1.01	0.301	-0.111

*as detected by X-ray diffraction measurements.

+T_A- temperature of 6 hour heat treatment, T_A= 273 refers to as-quenched sample.

++ Area is normalized to be 1.00 for amorphous $Y_{0.75}Fe_{0.25}$.

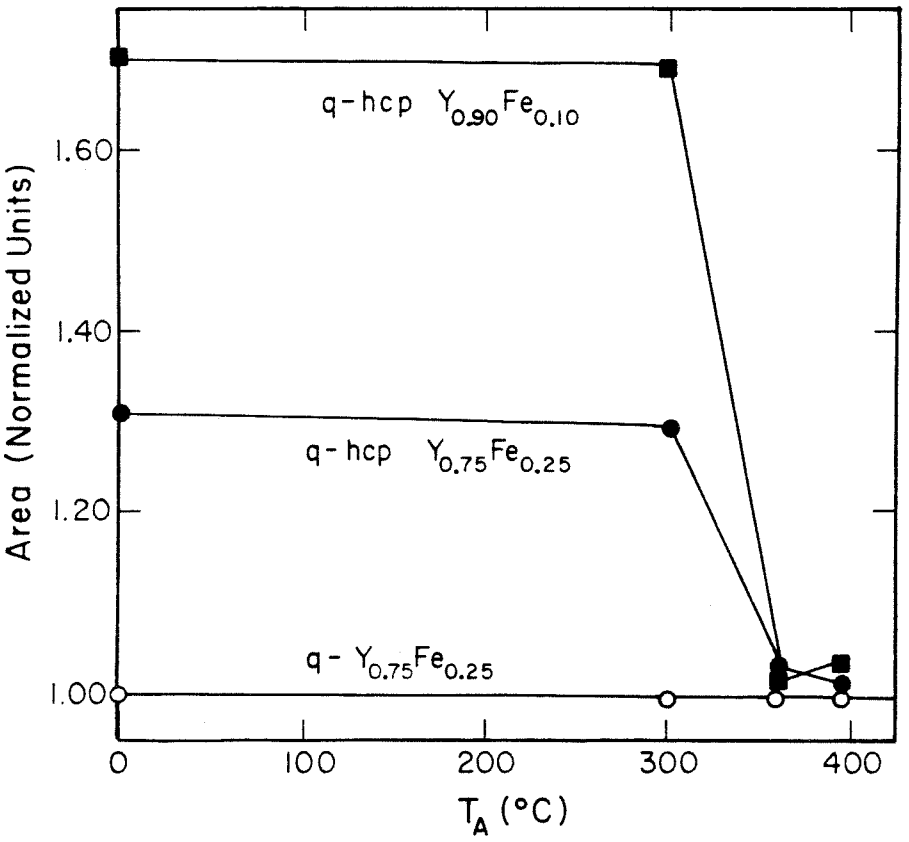

Fig. 26 Area under resonance of the ME spectra for amorphous $Y_{0.75}Fe_{0.25}$, q-hcp $Y_{0.75}Fe_{0.25}$, and q-hcp $Y_{0.90}Fe_{0.10}$ as a function of annealing for 6 hours at $T = T_A$. All measurements were made at room temperature.

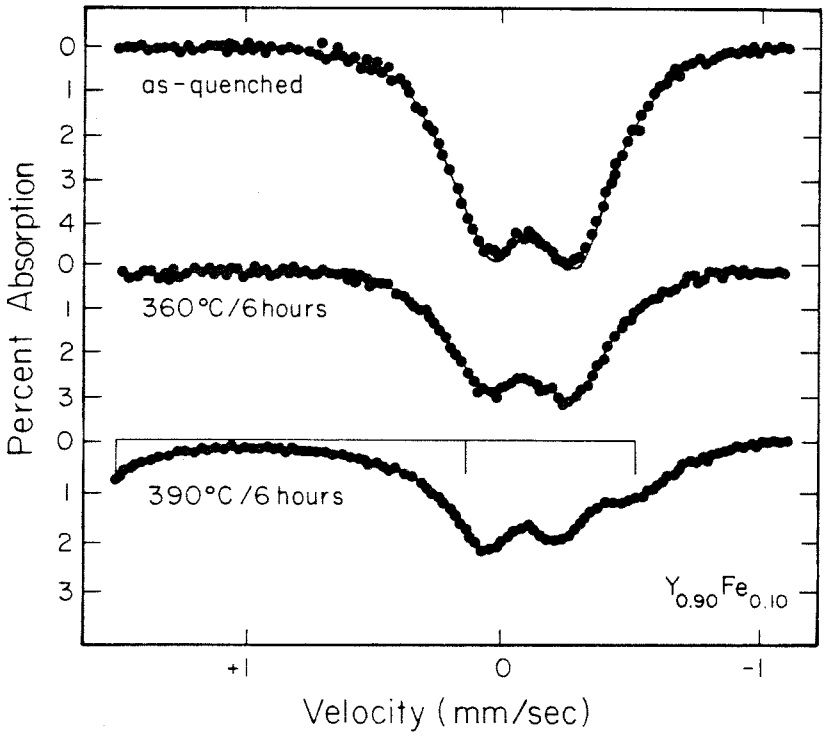

Fig. 27 ME spectra of the q-hcp $Y_{0.90}Fe_{0.10}$ sample for several heat treatments. The vertical bars above the lower spectrum show the positions and intensities of the contributions from Fe atoms in the C-15 compound.

that there are no significant differences in the behavior of QS or IS with T_A between the amorphous and q-hcp samples is somewhat puzzling. It may mean that the contribution to the ME spectra from the high f sites is poorly defined or perhaps similar to that of the amorphous phase. Knowing the contribution to the area from the high f site, we can estimate an effective Debye temperature for this site. We find that the Debye temperature of this site is about 700 K which reinforces our identification of this site as an interstitial one. For comparison, the effective Debye temperature of the amorphous phase is 270 K (the same as pure hcp Y).

The initial values of IS and QS for the partially crystalline samples of this study are somewhat surprising in view of our work on the crystallization of $Y_{0.66}Fe_{0.34}$. Concentrating on the q-hcp $Y_{0.90}Fe_{0.10}$ foil we see that its QS and IS correspond to a heat treatment of about 570 K/6 hours. From figs. 22 and 23 we estimate that the composition of the amorphous phase in this sample is approximately $Y_{0.50}Fe_{0.50}$.

We have shown that the X-ray and density measurements of Giessen et al on Y-Cu and Y-Fe cannot unambiguously show the existence of metal-metal solid solutions. We have also investigated a few ternary materials ($Y_{0.90}Cu_{0.10-z}Fe_z$ using the ME and we find that the interstitial solid solubility of Cu in Y is also much more restricted than Giessen et al had claimed. In both the Y-Fe and Y-Cu-Fe systems we find that the interstitial solid solubility is less than 3 at%. Our ME results on these systems are therefore the first clear demonstration of metal-metal interstitial solid solutions.

IV. DISCUSSION

We will begin this discussion with an analysis of the ME spectra of Fe impurities in the C-15 compounds YTM_2. In fig. 28 we show the unit cell of the C-15 structure(space group Fd3m). There are 8 Y and 16 TM atoms in the unit cell. The major skeleton is the diamond cubic network of Y atoms also shown in fig. 28. The smaller TM atoms are arranged in tetrahedra which are joined to each other at their vertices. This compound is chemically ordered in that the number of unlike neighbors is greater than a random arrangement of Y and TM atoms. Each Y atom has 4 Y and 8 TM near neighbors while each TM atom has 6 Y and 6 TM near neighbors. Like many other transition metal compounds, the C-15 phases are generally considered as size factor compounds. The ideal radius ratio(R_Y/R_{TM}) of the two constituents is 1.225. At this ratio there are Y-Y contacts but no Y-TM or TM-TM contacts. The criteria for deciding whether a contact is formed being that the distance in the crystal be less than the sum of the corresponding metallic radii. Y-TM contacts begin to form when $R_Y/R_{TM} > 1.34$. For the alloys of this study $R_Y/R_{TM} > 1.34$, so that both Y-Y and Y-TM contacts exist. In Table IX we list the structural data on these compounds derived from the X-ray diffraction experiments. Note that the metallic radius of Y(r_Y) is 0.18nm which means that d_{YTM} is just the sum of $r_Y + r_{TM}$ while d_{YY} is considerably smaller than $r_Y + r_Y$. Y forms the C-15 phase with Al, Co, Fe, Ir, Mn, Ni, Pt, and Rh. Of these, only Al is a simple(non-transition) metal. It is also interesting to note that metallic glasses can be formed in all

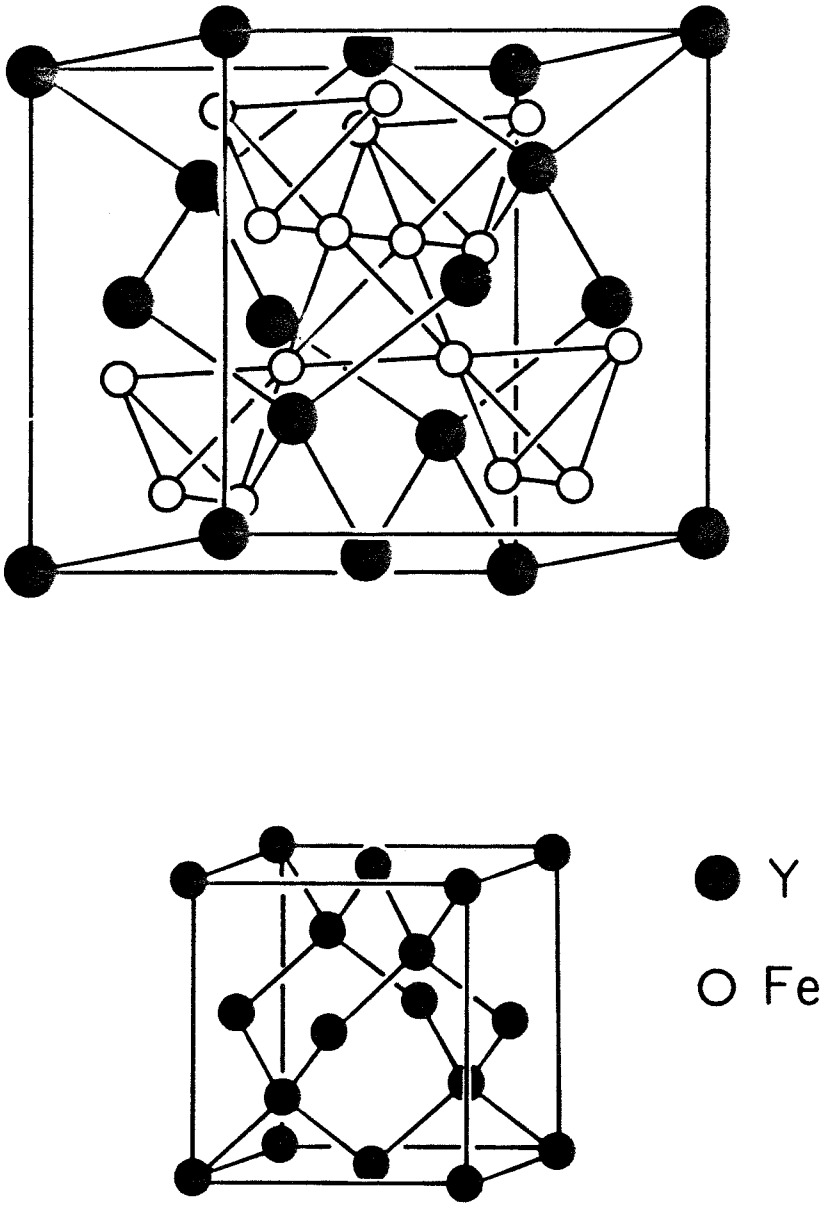

Fig. 28 (Top) Unit cell of the C-15 compound and (bottom) the Y sub-lattice.

Table IX Structural data for C-15 compounds.

Compound	a_o(nm)	d^*_{TMTM}(nm)	d_{YY}(nm)	d_{YTM}(nm)	R^+_{TM}(nm)	R_Y/R_{TM}
YMn_2	0.767	0.272	0.332	0.318	0.134	1.34
$Y(Fe_{0.50}Mn_{0.50})_2$	0.748	0.265	0.324	0.310	0.130	1.38
YFe_2	0.735	0.260	0.318	0.306	0.126	1.43
YCo_2	0.721	0.256	0.312	0.299	0.125	1.44
YNi_2	0.718	0.252	0.308	0.296	0.124	1.45

*d_{AB} is the distance between atoms A and B.

+R_A is the metallic radius of atom A assuming a coordination number of 12.

these binary systems. In our discussion of the $Y_{66}(Fe_yTM_{1-y})_{34}$ glasses we noted that there are similarities between the behavior of the M.E. parameters of these glasses and the corresponding C-15 compounds. We will now try to understand the IS and QS of Fe impurities in these materials.

We mentioned before that a convenient way to express the difference in IS between chemical environments is by the expression

$$\Delta IS = a\Delta n_d + b\Delta n_c + c\ \Delta V/V_o$$

The first two terms which represent changes in the d-electron and non-d-electron counts are related to the chemical identities of the atoms in the first nearest neighbor shell about the resonant atom. We will refer to these terms as the chemical part of the IS. These contributions must come from alloying effects and are determined to a large extent by the electronegativity difference between the resonant atom and the surrounding atoms and the nature of the bonds they form. In the YTM_2 alloys, we wish to discuss the changes in IS as the identity of TM is varied. The Y-Fe interactions are common to all these hosts so that the changes in the chemical part of the IS must come from changes in the Fe-TM interactions. The chemical part of the IS (the so-called volume corrected isomer shift) has been experimentally determined for dilute Fe impurities in a variety of transition metal hosts. The chemical part has been found to be

nearly independent of the structure of the host. In crystalline alloys such as Fe-Mn it varies linearly with the Fe content.[24] Thus, we can estimate the chemical part of the IS by using the volume corrected isomer shifts scaled for the number of TM neighbors. For Fe with 12 TM neighbors the chemical part of the IS is for the TM's of this study: Mn(-0.30 mm/sec), Fe(0.00 mm/sec), Co(+0.04mm/sec), and Ni(+0.09 mm/sec).[9]

The other contribution to the IS comes from changes in the atomic volume of the Fe site. From high pressure experiments on α-Fe, it has been found that the IS obeys the formula[25]

$$\Delta IS = (1.50 \pm 0.01 \text{ mm/sec}) \times (\Delta V/V_o)$$

When Fe is added to a crystalline material it experiences a compressive or expansive pressure depending on whether the atom it is replacing is smaller or larger. For the YTM_2 alloys for example, the Fe atoms are under expansion for TM=Mn and compression for TM=Co and Ni. One way to gauge the change in volume for the YTM_2 compounds is to simply use the change in volume of the unit cell.

In fig. 29 we have plotted the IS of the $Y(Fe_xMn_{1-x})_2$ samples as a function of Fe concentration. The solid line through the points is the calculated IS taking into account the chemical and volume terms as described above. We see that this scheme is in good agreement with the experimental values. In Table X we continue this kind of analysis for the various YTM_2 host alloys. This time

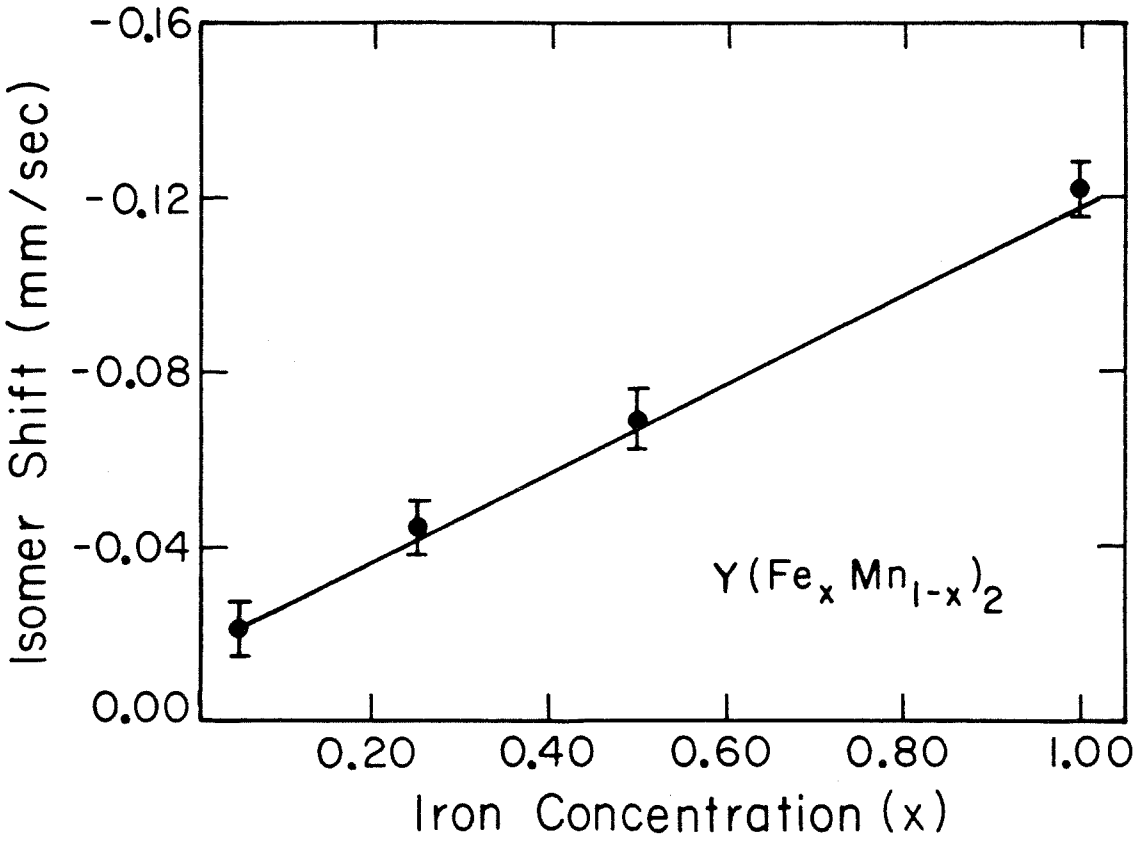

Fig. 29 IS values of the C-15 compounds $Y(Fe_xMn_{1-x})_2$. The points are the actual data points and the solid line is the prediction taking into account the chemical and volume contributions to the IS. The prediction is constrained to go through the point x=0.05.

Table X Comparison between the volume of Fe in $Y(Fe_xTM_{1-x})_2$ using ME and X-ray diffraction.

TM	x	IS* (mm/sec)	V^{+}_{eff} (from ME) (nm^3)	$V_{metallic\ radii}$ (nm^3)	$V_{X\text{-}ray}$ (from a_o) (nm^3)	V^{++}_{ME} (from ME) (nm^3)
Mn	0.05	+0.087(9)	9.97×10^{-3}	9.97×10^{-3}	0.454	0.454
Mn	0.25	+0.023	9.55(4)	9.59	0.436	0.434(2)
Mn	0.50	-0.037	9.17	9.17	0.419	0.416
Fe	1.00	-0.165	8.29	8.37	0.398	0.377
Co	0.05	-0.198	8.08	8.17	0.375	0.367
Ni	0.05	-0.218	7.96	7.96	0.370	0.361

*With chemical corrections.

+ Volume of Fe atom in YTM_2 host, fixing the value of the TM = Mn, x=0.05 case.

++Unit cell volume of YTM_2 host, fixing the value of the TM = Mn, x=0.05 case.

we correct the observed IS by the chemical term (IS^*) and calculate the volume of the Fe atoms in these hosts. We see that the atomic volumes for Fe derived from the ME data (V_{ME}) are in good agreement with the volumes calculated from the lattice parameters of compounds ($V_{X\text{-}ray}$) and the TM volumes estimated from the TM metallic radii. As we expected, when Fe substitutes for a TM atom in this structure it occupies the same volume the TM atom normally has.

The behavior of the QS's of the various YTM_2 hosts is a little more difficult to discuss. In the C-15 structure the Fe atoms are along a threefold symmetry axis (along the (111) direction) which means that $\eta = 0$ and the QS is determined by eq. The unit cell is cubic so that we can write all the atomic positions in terms of the lattice parameter (a). From this we might expect eq to be proportional to $1/a^3$. In Table XI we list the values of QS and $1/a^3$ for the YTM_2 hosts. We see that the changes in QS are much larger than the changes in $1/a^3$, so that this is not the most important factor determining QS. In Table XI we have also listed some of the structural data on these compounds. Comparing this to the QS data we see two important features. First, we see that when Fe replaces the smaller atoms Co and Ni the QS is large and when it replaces the larger atom Mn QS is small. Second, the QS is larger for larger values of R_Y/R_{TM}. We can understand these observations as being the result of a contribution to the QS coming from a local distortion of the atomic environments due to strain. We can in this case two mechanisms leading to strain. For $R_Y/R_{TM} > 1.34$ we saw that the Y-Y contacts are under

Table XI QS and structural data on C-15 compounds $Y(Fe_xTM_{1-x})_2$.

TM	x	QS (mm/sec)	$1/a_o^3$ (nm^{-3})	R_Y/R_{TM}	R_{TM}/R_{Fe}
Mn	0.05	0.218(7)	2.2	1.34	1.06
Mn	0.25	0.220	2.3	1.36	1.05
Mn	0.50	0.250	2.4	1.38	1.03
Fe	1.00	0.480	2.5	1.43	1.00
Co	0.05	0.466	2.7	1.44	0.99
Ni	0.05	0.553	2.7	1.45	0.98

compression and that this compression increases as R_Y/R_{TM} increases. It goes from 8% for YMn_2 to 14% for YNi_2. The other mechanism which can produce a distortion in the Fe environments is a size effect. This is the same kind of effect we described earlier for the volume dependence of IS. This case is different in that the QS is sensitive to the changing d-character of the Fe atomic orbitals as the pressure is changed. The important parameter is not the amount of d-character, but rather the symmetry of the d-orbitals and how this symmetry changes with pressure. It is not clear which of these is the dominant mechanism determining QS and it is likely both are involved. There is no simple experimental or theoretical way of separating the two contributions.

We will try to use the framework developed above to discuss the M.E. results on the various metallic glasses we have investigated. Let us begin this discussion by proposing a model for the arrangement of the atoms in these glasses and then examining the experimental results in the light of this model. We suggest that these glasses are chemically homogeneous but that there are regions of the glass which have a definite topological short range order. The size of these ordered regions is probably less than about 0.25 nm and they do not pack tightly together. In between these ordered regions we have Y and TM atoms in a disordered phase in which the TM atoms experience a wide variety of topological and chemical environments. We find that this simple model has all the ingredients necessary for us to understand the M.E. results. The Fe sites we referred to earlier as site 2 Fe

atoms are located in the ordered regions. Here the nature of the short range order about the Fe atoms is expected to be a function of composition and identity of the constituents of the glass. These Fe sites are expected to have many properties in common with the Fe sites in the C-15 YTM_2 compounds. The Fe sites we were calling site 1 are now identified as Fe atoms in the disordered phase and perhaps Fe atoms on the surface of the ordered regions. In other words, site 1 Fe atoms correspond to all the Fe atoms having a different local topology than the Fe atoms in the ordered phase. With this in model in mind we will now examine the ME data.

In the $Y_{1-x}Fe_x$ glasses(fig. 18) we saw that the IS and QS of site 2 changes around x=0.36. This indicates that both the chemical and topological short range order in the ordered phase has changed. From the crystallization studies we estimated that on the average, Fe has 4 nearest neighbor Fe atoms for this composition. The magnitude and direction of the change in IS-2 with x we see in fig. 18 corresponds to the substitution of one of the Y near neighbors by an Fe atom. This additional Fe neighbor changes the point symmetry about the Fe atoms. From the QS-2 data(fig. 18) we saw that the changes in QS-2 begin about x=0.34 and are completed by x=0.40. Assuming a 12-fold coordination of Fe and no chemical ordering between Y and Fe atoms we would expect that x=0.34 corresponds to 4.08 Fe neighbors and that x=0.40 corresponds to 4.80 Fe neighbors in agreement with our suggestions above. In fig. 18 we saw that site 1 does not experience a change in QS-1 with x, but that its IS-1 increases with x. The change in IS-1

indicates that the average number of Fe near neighbors is increasing much like that in the ordered phase. This fact is responsible for the symmetric nature of the spectra as x is changed. The independence of QS-1 with Fe content is expected for Fe environments lacking a definite topology.

For the $Y_{66}(Fe_{0.05}TM_{0.95})_{34}$ (TM = Mn, Co, Fe, and Ni) glasses we saw that the ME parameters of site 2 were sensitive to the identity of TM while the ME parameters of site 1 were less sensitive. We illustrate this fact in fig. 30 where we have plotted the IS's of site 1 and site 2 for the TM = Mn glasses as a function of Fe content. We see that the changes in IS-2 are very similar to those occurring in the crystalline alloys $Y(Fe_xMn_{1-x})_2$. As in the $Y_{1-x}Fe_x$ case, we can understand the lack of sensitivity in the site 1 parameters as being due to the poorly defined environments the Fe atoms experience in this phase. Earlier in this discussion we described the factors responsible for the IS and developed a simple scheme for understanding the IS in the YTM_2 alloys. We now apply the same ideas to the values of IS-2 for the $Y_{66}(Fe_{0.05}TM_{0.95})_{34}$ glasses. In this case we do not know the Fe-TM coordination number (N_{TM}) or the changes in volume caused by the various TM's. We will assume that the structure of the TM = Mn, Co, Fe, and Ni glasses are the same and find the volume of the Fe sites for several values of the Fe-TM coordination number (N_{TM}). We list the results of this procedure for the various glasses in Table XII.

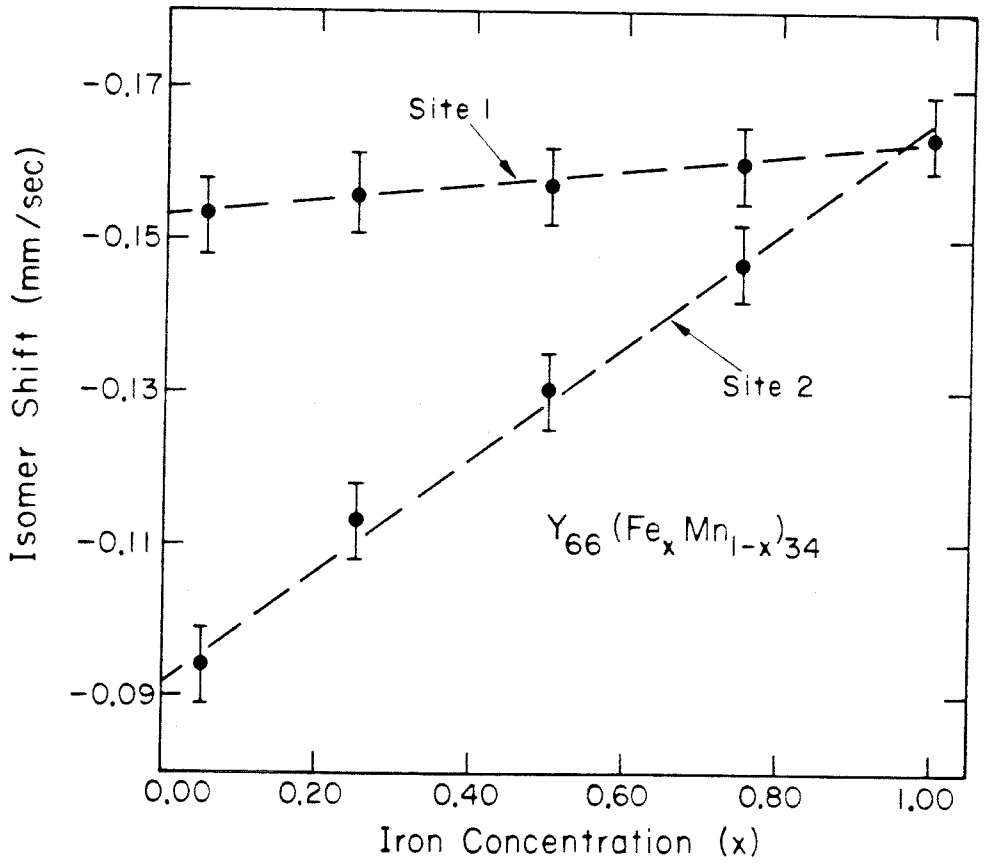

Fig. 30 IS values obtained by fitting the ME spectra of the $Y_{66}(Fe_xMn_{1-x})_{34}$ glasses to two sites plotted against the Fe concentration (x).

Table XII The effective volume (V_{eff}) of Fe atoms in $Y_{66}(Fe_{0.05}TM_{0.95})_{34}$ glasses for several values of N_{TM}.

TM	$V_{eff}(N_{TM}=2)$ (nm^3)	$V_{eff}(N_{TM}=4)$ (nm^3)	$V_{eff}(N_{TM}=6)$ (nm^3)	$V^*_{metallic\ radii}$ (nm^3)
Mn	9.05×10^{-3}	9.34×10^{-3}	9.63×10^{-3}	9.97×10^{-3}
Fe**	8.38	8.38	8.38	8.38
Co	8.34	8.29	8.21	8.17
Ni	8.34	8.21	8.13	7.96

*Volume calculated from the metallic radii of the TM's.

**The Fe volume in $Y_{0.66}Fe_{0.34}$ has been taken to be 8.38×10^{-3} (nm^3).

Note that unlike the YTM_2 hosts, we see in this case that V_{ME} is not equal to the TM volumes calculated from the metallic radii of the TM. This is perhaps not a surprising result and indicates that in contrast to the crystalline case, some relaxation of the atoms about the impurity Fe sites occurs in the glass.

The dependence of QS-2 with TM in these glasses is similar to the QS values of the YTM_2 hosts. We see that QS-2 is small when Fe replaces the larger atom Mn and it is large when it replaces the smaller atoms Co and Ni. The values of QS-2 and the changes we see as TM is changed are smaller than the case of the YTM_2 hosts. Like our discussion of QS in the YTM_2 hosts, it is tempting to relate QS-2 to the local strain introduced by the fact that Fe has a different size compared to the other TM's. Although this idea does seem to nicely fit the data we stress that there is little justification for believing it.

An important result of our work on the $Y_{66}(Fe_yTM_{1-y})_{34}$ glasses was the strikingly different behavior of the TM = Cu and Zn glasses compared to the TM = Mn, Fe, Co, and Ni glasses. From this we concluded that the structure of the TM = Cu and Zn glasses is somewhat different than the others. This observation demonstrates the importance of factors other than size in determining the structure of metallic glasses. If size were the only relevant factor involved in specifying the structure of the glass, then we would expect $Y_{66}Fe_{34}$, $Y_{66}Co_{34}$, $Y_{66}Ni_{34}$, and $Y_{66}Cu_{34}$ to be isostructural. Instead, we find that the Cu glass is very different from the others and that $Y_{66}Mn_{34}$, despite the larger

size of Mn, is similar to the Fe, Co, and Ni glasses. We think that it is significant that the TM= Mn, Fe, Co, and Ni glasses are isostructural since these are the 3d elements which form C-15 compounds with Y. In the Y-Fe and Y-Mn binary systems, these are the Y richest compounds. Referring back to Table IX we see that these C-15 compounds all have size ratios greater than the ideal ratio for this structure, which leads to a compression of the Y-Y contacts. The energy for this compression is provided by the formation of Y-TM bonds which occur for R_Y/R_{TM} greater than 1.34.[27] We see that size is not the only factor determining whether the C-15 compound is stable. The large negative heat of formation of Y-TM bonds is crucial to forming this structure whenever the size factors are not favorable. It is interesting to point out that Cu does not form any binary C-15 compounds with transition metals. In fact, the only binary Cu C-15 compound is $MgCu_2$ in which the size ratio is 1.25. As we noted before, Al is the only non-transition metal which forms the C-15 compound with Y. In this case,like that of $MgCu_2$, the size ratio(1.26) is almost the ideal value. From these comments we suggest that size is perhaps the most important factor determining whether the C-15 compound will form in a binary system when one of the components is a simple metal. For the case of transition metals, the compound can form even when the size factor is unfavorable provided there is a large heat of formation of Y-TM bonds. We believe that the failure of Cu and Zn to form the C-15 compound with Y may be that the energy needed to compress the Y atoms cannot be obtained by the formation of Y-Cu(Zn) bonds and may

indicate the importance of d-band binding for these compounds. Whatever the reasons are for Cu and Zn not forming C-15 compounds with Y, it seems likely that these same factors are responsible for the differences we see in the M.E. spectra between the TM=Cu and Zn and TM= Mn, Fe, Co, and Ni glasses.

Before we discuss the crystallization experiments, we must clear up the disagreement we noted between the TM = Fe and Mn crystallization experiments. We saw that the IS of the RAP saturates at a heat treatment of 633 K/6 hours in all of these systems. In the case of TM = Fe the final value of IS-a was higher that IS-c (YFe_2) while for the two TM = Mn glasses ($Y_{66}(Fe_yMn_{1-y})_{34}$, y=0.05 and 0.50) the final value of IS-a is lower than the corresponding C-15 compounds. The apparent discrepancy in these experiments is due to differences in the Fe environments in the TM = Mn glasses and crystals. We expect that the Fe environment in the 633 K/6 hours TM = Fe and Mn samples are similar and that the IS differences are related to the same volume and chemical terms we discussed above. We have already shown that the volume of an Fe atom in the crystalline C-15 compounds $Y(Fe_xMn_{1-x})_2$ is what you would expect to obtain from the metallic radii of Mn and Fe. As we pointed out, the situation in the amorphous samples is different because of relaxation about the impurity Fe sites. The atomic volume for Fe is smaller in the amorphous phases than in the corresponding crystals. If we assume that the Fe volumes in the RAP's are the same as in the as-quenched glasses, then we can estimate the change in the number of Fe-TM neighbors due to heat treatment. We find for the two compositions studied that the number of Fe-TM neighbors in the RAP's is approximately 8. This

is illustrated in Table XIII. This number is in agreement with our estimate from the Y-Fe crystallization studies based on comparing the RAP to the changes in the YFe_2 compound with annealing. We see that the TM = Mn and Fe experiments agree and that our estimate above reinforces the conclusion that the Fe atoms in the RAP have about 2 more TM near neighbors than the Fe atoms in the C-15 hosts. This suggest that the amorphous phase is not chemically ordered.

With this point straightened out we now turn to a discussion of the crystallization process of the Y-Fe-Mn glasses. We saw that the formation of hcp Y is intimately related to the movement of Fe atoms in the sample. The changes in IS indicate that the amorphous phase left behind as hcp Y is formed becomes richer in Fe as T_A increases. From the comparison of the two site fits of as-quenched and samples composed of hcp Y and the RAP we saw that the number of Fe atoms in the ordered phase (site 2) increases while the number of Fe atoms in the disordered phase (site 1) decreases with annealing. A description of the process of the formation can be given with the above comments in mind.

We imagine that the as-quenched glass is chemically homogeneous and the formation of hcp Y crystalline nucleii requires the diffusion of both Y and Fe atoms. The disordered nature of the atoms in the site 1 phase apparently makes it easier for the Fe atoms to diffuse out of these regions. In addition, the ordered phase is also changing composition which requires the diffusion of Y from these regions. We imagine that the Y crystals form and start growing in the disordered phase. The Fe atoms originally in this phase either begin to form

Table XIII IS values for heat treated $Y_{66}(Fe_yMn_{1-y})_{34}$ glasses.

y	Condition	IS-2 (mm/sec)	IS-2* (mm/sec)	N_{TM}^{**}
0.05	as-quenched	-0.094(8)	-0.259	-
0.05	RAP + hcp Y	-0.122	-0.287	7.4
0.05	C-15 + hcp Y	-0.020	-0.272	6.0
0.50	as-quenched	-0.131	-0.216	-
0.50	RAP + hcp Y	-0.126	-0.211	8.5
0.50	C-15 + hcp Y	-0.069	-0.197	6.0
1.00	as-quenched	-0.165	-0.165	-
1.00	RAP + hcp Y	-0.104	-0.104	-
1.00	C-15 + hcp Y	-0.122	-0.122	6.0

* After volume correction.

** Estimated from the condition that the IS of the Mn and Fe systems should be the same after the appropriate chemical and volume corrections have been made. For C-15 compounds, N_{TM} is 6.0.

additional ordered regions or become part of the existing ordered regions. Y atoms orginally in the ordered regions have some probability of diffusing to the hcp Y phase and becoming part of it. This exchange of Y and Fe atoms will continue until the distance the atoms have to diffuse to reach the appropriate phase becomes too large. At this point, the sample reaches a metastable state consisting of amorphous regions surrounded by hcp Y crystals. The X-ray diffraction pattern of such a sample was shown in fig. 20. We saw only the broad Bragg peaks corresponding to hcp Y in these kinds of samples. This is an important point for our discussion of the Zr-Hf-V samples in the final section. The activation energy we deduced for the formation of hcp Y (Δ_1) should be interpreted as some kind of average energy associated with the diffusion of Y and Fe atoms in the sample. We see that this is not a well defined quantity.

As we mentioned before, we believe that the composition of the RAP is about 66 at% Fe. If this is true then the formation of YFe_2 from this phase simply requires the topological rearrangement of the atoms. The fact that the IS of the RAP does not change during the formation of the YFe_2 crystals supports this idea. The rearrangement of the atoms to form the YFe_2 crystals is reflected in the large difference we see between QS of the C-15 compound and the QS of the RAP.

We see that the simple model of having ordered and disordered regions in the glass allows us to understand the ME data in a consistent manner. Lets us return to our original description and explain some of

the details of this model. The terms phases or regions we used are perhaps inappropriate. The ME experiments give us information primarily on the first near neighbor shell about the resonant atom. We have no direct information on the extent of the so-called ordered region. The so-called disordered regions are even more of a mystery. It is clear from our experiments that the disordered region represents a number of different Fe environments. It seems to have the same average composition as the ordered regions, although we expect that the fluctations in the Fe-TM coordination number is higher in these regions. Our statement that the glasses are chemically homogeneous therefore requires some further explanation. It is chemically homogeneous in the sense that the average composition of the two regions is the same. On a microscopic scale, we see that the Fe atoms in the ordered regions have a N_{TM} that is well defined. In $Y_{1-x}Fe_x$, for example, we believe that N_{TM} is 4 for $Y_{0.68}Fe_{0.32}$ and 5 for $Y_{0.60}Fe_{0.40}$. For a composition in between these, there are some Fe atoms with $N_{TM} = 4$ and some with $N_{TM} = 5$. In contrast, we might describe the N_{TM} of the disordered phase by something like a binomial distribution; keeping the total coordination number (Y + TM) constant at 12.

A variety of models have been proposed to describe the structure of metallic glasses. The comparisons between the models and the actual structure of the glass are made by determining the pair correlation functions of the two. For the case of the glass the pair correlation functions are determined by one of, or combinations of the diffraction techniques. One of the most successful models is the dense random

packing of hard spheres (DRPHS) model based on the investigations of Bernal.[28] For the metal-metalloid glasses (e.g. $Pd_{80}Si_{20}$) a reasonable first approximation to the structure of the glass is to assume a dense random packing of Pd atoms and to incorporate the Si atoms in the "holes" of this packing. The Si atoms are packed in the structure with the restriction that there be no Si-Si first near neighbors. For the metal-metal glasses (e.g. Y-Fe) the approach has been to use a binary DRPHS model.[29] This approach has not been very successful and serious problems exist concerning the density of such models.

We should point out that the diffraction techniques would not be sensitive to the two kinds of Fe regions in these glasses since their information is an average over all Fe environments. They would also not be able to distinguish the different topologies we see for the different regions. We would expect, for example that the pair correlation functions for the $Y_{66}Cu_{34}$ and $Y_{66}Fe_{34}$ glasses to be nearly identical. Only a microscopic probe can distinguish between the very different structures of these glasses. In this study we have found that the ME can provide information on very complicated materials. The information we obtained on the RAP's and the interstitial Fe sites, for example, could not have been obtained by any of the diffraction techniques.

The remarkable differences we saw in the ME spectra for the TM = Mn, Fe, Co, and Ni and TM = Cu and Zn glasses indicate that simple hard sphere models are inappropriate here. The directional bonding we expect from the transition elements Mn, Fe, Co, and Ni must somehow

be incorporated into the model. A simple extension of the DRPHS model would be to use asymmetric balls to represent Mn, Fe, Co, and Ni and perhaps symmetric balls to represent the Cu and Zn atoms.

Our ME results suggest an interesting approach to modeling the structure of the Y-Fe glasses. We can imagine randomly packing the objects we called the ordered regions together and filling in the gaps left by this packing with atoms arranged in a very disordered manner. Unfortunately, our experiments are not able to determine the input parameters of such a model (size and shape of the ordered units). There is also the problem of comparing the model with something we know about the glass.

V. APPLICATION

As an interesting application of our study of the crystallization of the Y-Fe glasses we will briefly mention our work on the related glasses Hf-Zr-V.[30,31] The equilibrium phase diagram of the Hf-V and Zr-V systems are very similar to that of Y-Fe. For Hf(Zr) rich compositions the equilibrium phases are hcp Hf(Zr) and the C-15 compound $Hf(Zr)V_2$. The C-15 compounds of these ternary materials are excellent crystalline superconductors. The maximum value of the superconducting transition temperature (T_c) is about 10 K and the maximum of the upper critical magnetic field (H_{c2}) at 4.2 K is about 250 kOe. These compounds, like all other crystalline high field superconductors, are very brittle. This brittleness prevents the easy fabrication of superconducting devices.

We found that metallic glasses can be obtained by rapid quenching in the Hf-V, Zr-V and (Hf-Zr)-V systems. The as-quenched glasses have excellent mechanical properties (flexibility and ductility), but are not superconducting above 1.5 K. Fully crystallized foils have values of T_c and H_{c2} comparable to as-cast samples. The crystallization of these glasses appears to be very similar to that of Y-Fe,and heat treatments dramatically improve the superconducting properties of the materials.

In fig. 31 we show the results of critical current density (J_c) measurements on partially crystalline samples of $(Zr_{0.75}Hf_{0.25})_{60}V_{40}$. In these measurements the critical current is defined as the maximum

current that can flow through the sample at a given temperature and applied magnetic field with a voltage drop across the sample of less than 1 μV. Concentrating on the $(Zr_{0.70}Hf_{0.30})_{60}V_{40}$ samples we see that the 600°C/72 hours heat treatment sample carried more current than the 1000°C/72 hours sample for all values of $H_{applied}$. This difference is greater at high fields, for example, at $H_{applied}$ = 150 kOe, J_c of the 600°C/72 hours sample is two orders of magnitude higher than that of the 1000 C/72 hours sample. This is a somewhat surprising result since X-ray diffraction analysis of the samples showed that we had formed more of the C-15 compound in the 1000°C/72 hours sample. Since the T_c and H_{c2} of the two samples are similar the difference in their J_c's reflects the difference in their flux pinning force densities. From X-ray diffraction experiments on these samples we found that the effective size of the microcrystals formed by the heat treatments are 20 nm for the 600°c/72 hours sample and about 200 nm for the 1000°C/72 hours sample. We suggest that the very fine grain size which exists in the 600°C/72 hours sample is responsible for the observed J_c enhancement. Further support for this explanation is obtained by comparing the J_c versus $H_{applied}$ of the 600 C/72 hours sample and the data from ref. 32 on arc melted $(Zr_{0.50}Hf_{0.50})V_2$ which presumably has a very large grain size. We see that for $H_{applied}$ = 180 kOe the 600°C/72 hours sample has a larger J_c than the arc melted sample. At 150 kOe we have nearly two orders of magnitude higher J_c for the 600°C/72 hours sample compared to the arc melted alloy. We should point out that the H_{c2} of the arc melted sample is higher than our sample due to its higher Hf content. This fact is

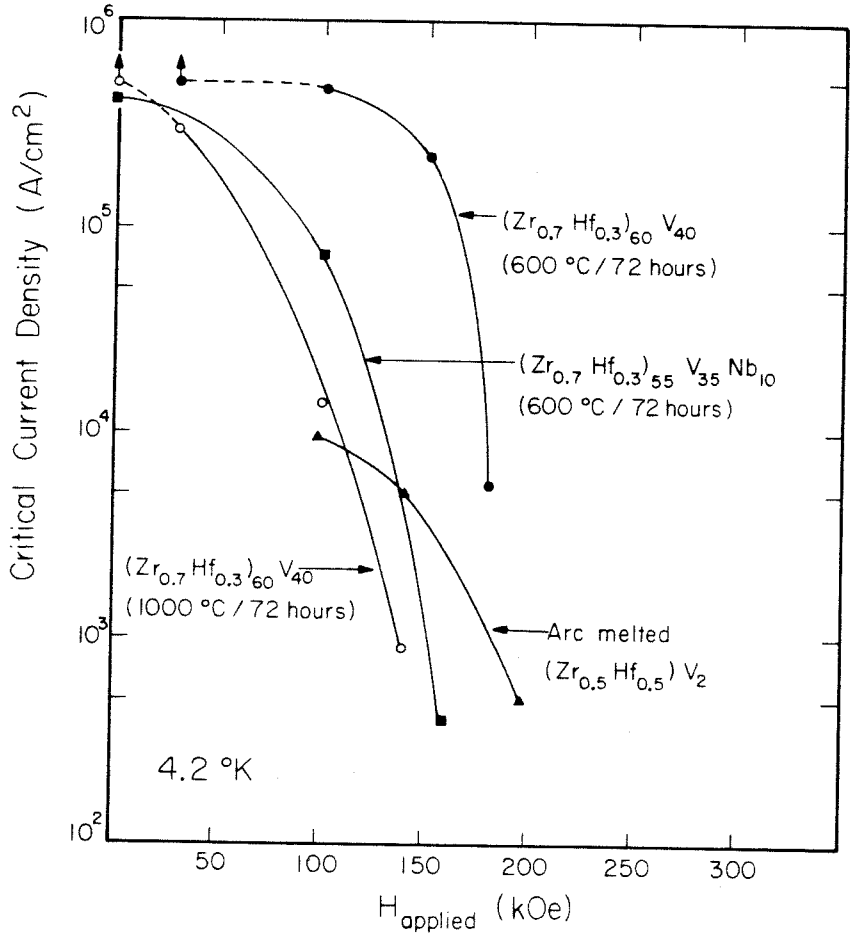

Fig. 31 J_c versus $H_{applied}$ for several Zr-Hf-Nb-V samples. In parentheses below the compositions are listed the heat treatments. The data for the arc melted sample are from ref. 32. All measurements are at 4.2 K. Upward pointing arrows on some of the points indicate that J_c was higher than we could measure.

responsible for its higher J_c at very high fields. From our description of the crystallization of Y-Fe glasses we can understand why the microstructure formed by annealing the Zr-Hf-V glasses is so conducive to high J_c's and large flux pinning force densities.

The first step in the process of crystallization is the formation of hcp Hf(Zr) at about 500°C. As the hcp phase is formed the remaining amorphous phase becomes richer in V. The hcp crystals can grow in size until the amorphous phase about them becomes so rich in V that further removal of Hf(Zr) in kinetically forbidden. When the V content of the remaining amorphous phase reaches about 66 at%, crystals of the C-15 compound will begin to form. Their size is limited by the surrounding crystals of hcp Hf(Zr). We thus form a very refined microstructure consisting of small regions of a good superconducting phase (the C-15 compound) embedded in a non-superconductor. The mechanism of flux pinning in such a system is related to the difference in free energy between having the fluxoids pass through the superconducting and non-superconducting regions of the sample. For optimum pinning the size of the regions should be a few times the coherence length of the superconducting phase. The coherence length of the C-15 superconductors is on the order of 5 nm. The high density of flux pinning sites resulting from the novel microstructure of the heat treated glasses is responsible for the dramatic improvement in the critical current densities in these materials compared to samples prepared by conventional techniques. We found that the superconducting properties of the C-15 compound we formed by heat treating the glasses had the same T_c and

H_{c2} as the as-cast alloys. This is an important observation since it allows us to estimate the size of the C-15 regions formed by the low temperature heat treatment. We know that the C-15 regions must be at least as big as the coherence length of the C-15 phase (about 5 nm), otherwise the T_c of this phase would be depressed by the proximity effect.[33] From the high values of J_c for the 600°C/72 hour sample we suspect that the regions are not much larger than about 15 nm.

The results of the J_c's of crystallized Hf-Zr-V glasses are potentially very important. The J_c versus $H_{applied}$ curves show that these materials are comparable to the best Nb_3Sn and V_3Ga conductors. By producing an amorphous phase in this system we can obtain a material in a useful form (ribbon, filaments, powder) having excellent mechanical properties. The idea is to fabricate the superconducting device (magnet, transformer, geneator etc.) using the material in its mechanically desirable amorphous form and to follow this with an appropriate heat treatment to produce the final material.

References

1) Frankfort H The Birth of Civilization in the Near East. (Doubleday, New York) (1956).

2) Duwez P and Willens R H Trans. Met. Soc. AIME 227 362 (1963).

3) Cargill G S Solid State Physics 30 227 (1975).

4) Hayes T M, Allen J W, Tauc J, Giessen B C, and Hauser J J Phys. Rev. Lett. 40 1282 (1978).

5) Stern E, Rinaldi S, Callen E, Heald S, and Bunker B Jour. of Mag. and Magnet. Mat. 7 188 (1978).

6) Mössbauer R L Z. Physik 151 124 (1958).

7) Breit G and Wigner E Phys. Rev. 49 519 (1936).

8) Wertheim G K Mössbauer Effect: Principles and Applications (Academic Press Inc. New York) (1964).

9) Watson R E and Bennett L H Phys. Rev B 17 3714 (1978).

10) Sharon T E and Tsuei C C Phys. Rev B 5 1047 (1972).

11) Giessen B C, Attard A E, and Ray R Proc. 2nd Int. Conf. on Rapidly Quenched Metals (M.I.T.) (1975).

12) Giessen B C, Madhava M, Polk D E, and Vander Sande J Mat. Sci. and Eng. 23 145 (1976).

13) Sitek J, Prejsa M, Cirak J, Hucl M, and Lipka J Jour. of Non-Cryst. Solids 28 225 (1978).

14) Boolchand P, Triplett B B, Hanna S S, and deNeufville J Mössbauer Effect Metholodology 9 (1974).

15) Boolchand P, Tenhover M, and deNeufville J Proc. 6th Int. Conf. on Amor. and Liq. Semiconductors (Leningrad) (1976).

16) Kim C S and Boolchand P Phys. Rev. B 19 3187 (1979).

17) Boolchand P, Tenhover M, and Flasck R E, AIP Conf. Proc. No. 31, Structure and Excitations of Amorphous Solids (AIP, New York) (1976).

18) Tenhover M, Boolchand P, and Bresser W to be submitted to Jour. of Non-Cryst. Solids (1981).

19) Duwez P Progress in Solid State Chemistry (Pergamon Press, Oxford) 3 377 (1966).

20) Condon E U and Shortley G H The Theory of Atomic Spectra (Cambridge University Press, Cambridge) (1953).

21) Steiner W Jour. of Mag. and Magnet. Mat. 14 47 (1979).

22) Giessen B C, Ray R, and Hahn S H Phys. Rev. Lett. 26 509 (1971).

23) Flinn P A, Gonser U, Grant R W, and Housely R M Phys. Rev. 157 538 (1967).

24) Kimball C, Gerber W D, and Arrott A J. Appl. Phys. 34 1046 (1963).

25) Pound R V, Benedek G B, and Drever R Phys. Rev. Lett. 7 405 (1961).

26) Teatum E, Gschneidner K, and Waber J LA 2345 U.S. Dept. of Commerce Washington D.C. U.S.A.

27) Pearson W B Acta. Cryst. B24 7 (1968).

28) Bernal J P Nature (London) 183 141 (1959).

29) Cargill G S and Kirkpatrick S AIP Conf. Proc. No. 31, Structure and Excitations of Amorphous Solids (AIP, New York) (1976).

30) Tenhover M Appl. Phys. 21 279 (1980).

31) Tenhover M IEEE Tranactions on Magnetics 17 1021 (1981) and Proc. of Appl. Superconductivity Conf. (Santa Fe 1980).

32) Inoue K, Tachikawa K, Iwasa Y Appl. Phys. Lett. 18 235 (1971).

33) Silvert W and Singh A Phys. Rev. Lett. 28 222 (1972).